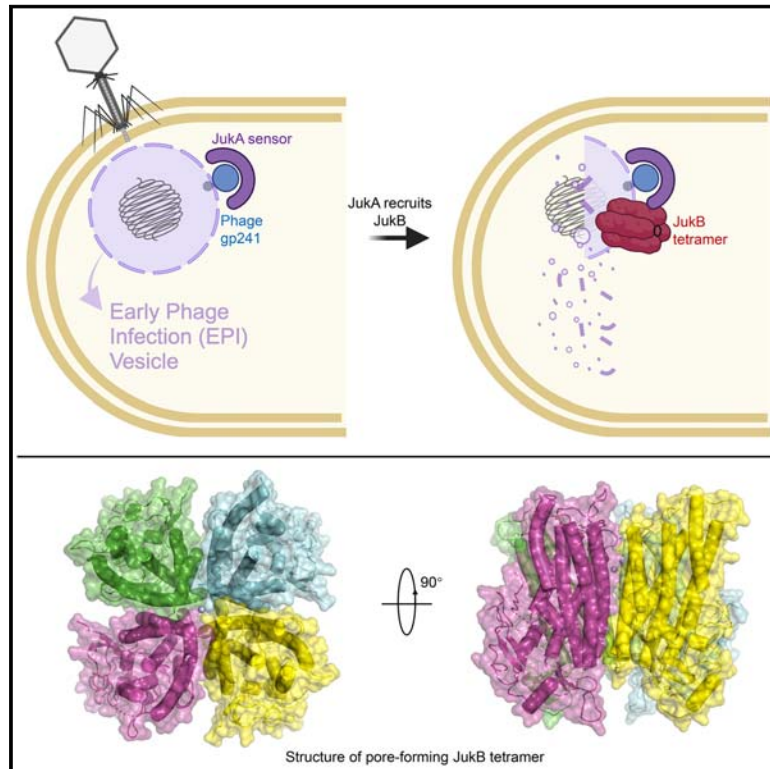


Jumbo phage killer immune system targets early infection of nucleus-forming phages

Graphical abstract



Authors

Li Yuping, Linlin Guan, Isabelle Becher, ..., Eugene V. Koonin, Yue Feng, Joseph Bondy-Denomy

Correspondence

yuping.li@unibas.ch (L.Y.),
fengyue@mail.buct.edu.cn (Y.F.),
joseph.bondy-denomy@ucsf.edu
(J.B.-D.)

In brief

Jumbo phage killer (Juk) system, a common bacterial immune system in Proteobacteria, recognizes and targets the early phage infection vesicle specific to ϕ KZ-like jumbo phages, terminates phage infection, and saves the bacterial cell.

Highlights

- Discover “jumbo phage killer” immunity specifically targeting ϕ KZ-like jumbo phages
- Sensor JukA binds an early-expressed phage protein and directly recruits JukB effector
- JukB forms tetrameric pores to destabilize early phage infection vesicle, limiting early expression
- Sensor JukA is widespread across bacterial phyla, coupled with diverse effectors



Article

Jumbo phage killer immune system targets early infection of nucleus-forming phages

Li Yuping,^{1,7,*} Linlin Guan,² Isabelle Becher,³ Kira S. Makarova,⁴ Xueli Cao,² Surabhi Hareendranath,¹ Jingwen Guan,¹ Frank Stein,³ Siqi Yang,² Arne Boergel,³ Karine Lapouge,³ Kim Remans,³ David Agard,⁵ Mikhail Savitski,³ Athanasios Typas,³ Eugene V. Koonin,⁴ Yue Feng,^{2,*} and Joseph Bondy-Denomy^{1,6,8,*}

¹Department of Microbiology and Immunology, University of California, San Francisco, San Francisco, CA 94403, USA

²State Key Laboratory of Green Biomanufacturing, College of Life Science and Technology, Beijing University of Chemical Technology, Beijing 100029, China

³European Molecular Biology Laboratory (EMBL), Meyerhofstraße 1, 69117 Heidelberg, Germany

⁴Computational Biology Branch, Division of Intramural Research, National Library of Medicine, National Institutes of Health, Bethesda, MD 20894, USA

⁵The Chan-Zuckerberg Institute for Advanced Biological Imaging and the Department of Biochemistry, University of California, San Francisco, San Francisco, CA 94143, USA

⁶Quantitative Biosciences Institute, University of California, San Francisco, San Francisco, CA 94403, USA

⁷Present address: Biozentrum, University of Basel, Basel 4056, Switzerland

⁸Lead contact

*Correspondence: yuping.li@unibas.ch (L.Y.), fengyue@mail.buct.edu.cn (Y.F.), joseph.bondy-denomy@ucsf.edu (J.B.-D.)

<https://doi.org/10.1016/j.cell.2025.02.016>

SUMMARY

Jumbo bacteriophages of the ϕ KZ-like family assemble a lipid-based early phage infection (EPI) vesicle and a proteinaceous nucleus-like structure during infection. These structures protect the phage from nucleases and may create selective pressure for immunity mechanisms targeting this specific phage family. Here, we identify “jumbo phage killer” (Juk), a two-component immune system that terminates infection of ϕ KZ-like phages, suppressing the expression of early phage genes and preventing phage DNA replication and phage nucleus assembly while saving the cell. JukA (formerly YaaW) rapidly senses the EPI vesicle by binding to an early-expressed phage protein, gp241, and then directly recruits JukB. The JukB effector structurally resembles a pore-forming toxin and destabilizes the EPI vesicle. Functional anti- ϕ KZ JukA homologs are found across bacterial phyla, associated with diverse effectors. These findings reveal a widespread defense system that specifically targets early events executed by ϕ KZ-like jumbo phages prior to phage nucleus assembly.

INTRODUCTION

The viruses that infect bacteria evolved numerous strategies to ensure faithful replication, assembly, and host lysis in an exquisitely timed manner. Conversely, bacteria employ a suite of diverse defense pathways to prevent phage adsorption or DNA ejection, target phage nucleic acid, or sense phage proteins and prevent phage spread by inducing cell death or dormancy.^{1–4}

A staggering phage diversity exists in the biosphere, driving the requirement for numerous, diverse immune pathways, and conversely, phages evolved diverse anti-immune mechanisms. Jumbo phages (that is, those with genomes >200 kb) of the ϕ KZ-like family possess many interesting attributes including pan-resistance to known DNA-targeting immune systems.^{5,6} Phages of this family assemble a membrane-bound “early phage infection (EPI) vesicle” at the start of the infection where early transcription occurs (from 0 to 15 min post-infection).^{7–11} These phages subsequently build a proteinaceous nucleus-like struc-

ture, which houses phage genome replication and middle/late transcription.^{10–13} Phage mRNA is likely exported out of the EPI vesicle and the phage nucleus and is translated in the bacterial cytoplasm.^{9,12,13} RNA-targeting CRISPR systems and engineered nucleases that bypass the nucleus barrier can stop phage propagation, but DNA-targeting CRISPR systems or restriction endonucleases cannot.^{5,6,14} RNA-targeting CRISPR systems are relatively rare and are not endogenously present in *Pseudomonas aeruginosa* (*P. aeruginosa*),^{15,16} the host for the best studied jumbo phage, ϕ KZ. Therefore, it remains unclear how *P. aeruginosa* and most other hosts infected by ϕ KZ-like phages antagonize phages with these protected replication mechanisms.

Here, we identify “jumbo phage killer” (Juk), a widespread immune system that specifically detects ϕ KZ-like jumbo phages early in infection, blocks phage replication, and saves the cell. Juk consists of a broadly conserved sensor (JukA, previously YaaW) that specifically recognizes a phage early protein (gp241) and a variable effector, JukB. JukA, JukB, and the



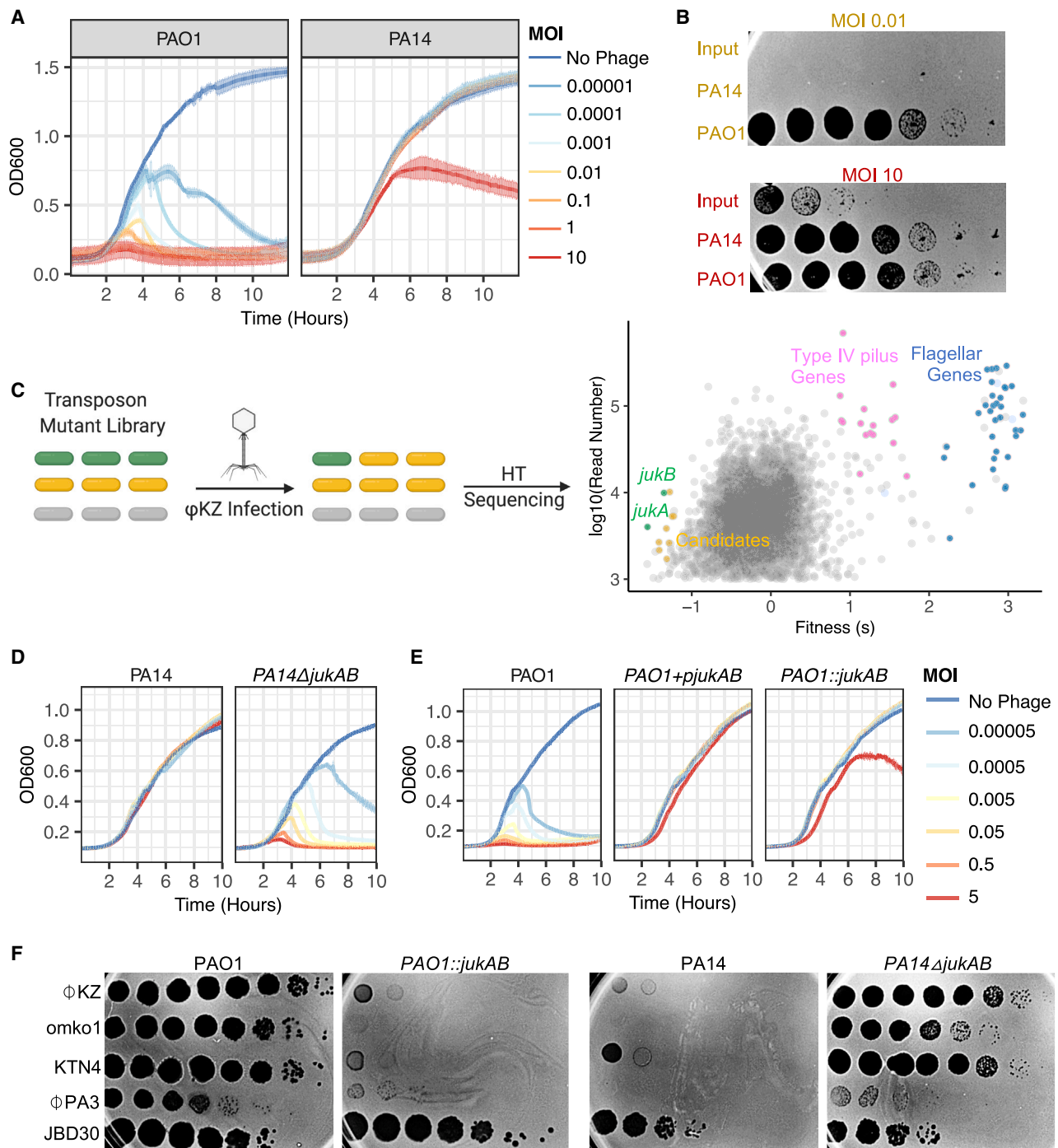


Figure 1. Discovery of the jumbo phage killer (Juk) system

(A) Bacterial growth curves (OD600) of *Pseudomonas aeruginosa* isolate PAO1 or PA14 across a range of multiplicities of infection (MOIs) of ϕ KZ. Error bars in (A) represent one standard deviation calculated from three technical replicates.

(B) Spot titration of ϕ KZ input and output (10 fold serial dilutions) from PAO1 or PA14 infection at MOI 0.01 or MOI 10 (from A) on a lawn of sensitive bacteria PAO1.

(C) Cartoon schematic of how the PA14 transposon (Tn) mutant library was constructed and used to identify ϕ KZ sensitive or resistant mutants. Each dot represents the Tn disruption of a unique gene. The fitness and read depth of Tn mutants are shown after being exposed to ϕ KZ. Genes of interest are highlighted. Fitness (s) is calculated as $\ln(\text{mutant frequency with } \phi\text{KZ infection}) / \ln(\text{mutant frequency without } \phi\text{KZ infection})$.

(legend continued on next page)

triggering phage protein form a complex that interferes with core functions facilitated by the EPI vesicle. In various microbial genomes, JukA is flanked by or fused to diverse putative effectors, including phospholipases and genes of unknown function.

RESULTS

Discovery of an immune system specifically targeting ϕ KZ-like nucleus-forming jumbo phages

To identify putative immune systems responsible for host resistance to ϕ KZ infection, we infected a panel of 62 *P. aeruginosa* clinical isolates under liquid infection conditions. About 50% of the tested isolates were resistant to ϕ KZ infection (Figure S1A). Such resistance could be caused either by the absence of bacterial factors, such as receptors, that are required for ϕ KZ infection or by the presence of immune mechanisms targeting key steps of the ϕ KZ infection cycle. Among the resistant strains, the model clinical isolate PA14 drew our attention because the strain grew well across a wide range of multiplicities of infection (MOIs), but its growth was inhibited at MOI >5 (Figures 1A and 1D). This growth inhibition of PA14 was caused by ϕ KZ replication (MOI 10 in Figure 1B), which did not occur at lower MOIs (MOI 0.01 in Figure 1B). In contrast, the growth of the phage-sensitive strain PAO1 was inhibited by ϕ KZ replication at MOIs as low as 10^{-5} (Figure 1A). The resistance of PA14 against lower MOIs implies that this strain possesses unknown immune mechanisms that can be overwhelmed at high MOIs.

To discover immune genes responsible for ϕ KZ resistance in PA14, a pooled PA14 transposon (Tn) mutant library was constructed, infected with ϕ KZ, and subjected to next-generation sequencing to identify Tn insertions (Figure 1C). Mutants with disrupted immune components would be sensitized to ϕ KZ infection whereas mutants lacking genes required for ϕ KZ propagation would resist infection. Disruption of flagellar and type IV pilus genes led to increased resistance (Figure 1C), suggesting that both structures are required for ϕ KZ infection.¹⁷ Phage adsorption assays confirmed that in *fliF:Tn* (flagellum) mutants, phage attachment was abolished (Figure S1B).

Our TnSeq data analysis identified 10 candidate genes, the disruption of which may lead to increased phage sensitivity (Figure 1C). Out of these 10 genes, 9 were present in the arrayed PA14 Tn-mutant library.¹⁸ These nine mutant strains were subjected to infection with ϕ KZ, revealing that Tn insertions in only two genes, *PA14_03360* and *PA14_03350*, showed changed sensitivity toward ϕ KZ infection (green dots in Figure 1C). *PA14_03360* and *PA14_03350* comprise a predicted two-gene operon; hereafter, we refer to these as Juk genes *jukA* and *jukB*, respectively. Deletion of either of these genes sensitized PA14 to ϕ KZ infection (Figures 1D and S1C), which could be complemented in *trans* (Figure S1C), suggesting that both *jukA* and *jukB* are required for immunity against ϕ KZ. When introduced into the ϕ KZ-sensitive strain PAO1 as a single copy with its native pro-

motor, *jukA* and *jukB* together (*PAO1::jukAB*), but not either gene alone, conferred resistance against ϕ KZ (Figures 1E and S1D). When present on a plasmid in PAO1 (*PAO1+pjukAB*), *juk* mRNA levels were ~ 10 -fold higher than in *PAO1::jukAB*, which further enhanced immunity and cell growth, indicative of a non-abortive mechanism (MOI 5 in Figure 1E). Collectively, our data demonstrate that the two-gene *juk* operon is necessary and sufficient to provide resistance against ϕ KZ infection.

To test the specificity of the Juk immune system, we conducted phage infection assays with a panel of phages from 12 different phage families (Figure S2A). In addition to restricting the growth of ϕ KZ, Juk also blocked the closely related phage omko1¹⁹ and KTN4²⁰ (10^{-6} efficiency of plating or EOP) and displayed weak protection against ϕ PA3²¹ (10^{-3} EOP) (Figure 1F). Omko1, KTN4, and ϕ PA3 belong to the ϕ KZ-related phage family and form a nucleus during infection. By contrast, Juk did not target the unrelated jumbo phage PA5oct (Figure S2A) or any other phage tested (e.g., JBD30 in Figure 1F), including 25 phages from 12 families (Figure S2A). Thus, Juk immunity appears to be specific toward ϕ KZ-related, nucleus-forming jumbo phages. Note that the reduced plaquing of ϕ PA3 on *PA14 Δ jukAB*, compared with on PAO1, could be caused by poor adsorption on PA14 strains (Figure 1F).

Juk system does not act via known immune mechanisms

HHpred search using JukA sequence (GenBank: WP_003137196.1) as a query identifies similarity with eukaryotic mitochondrial chaperones involved in the assembly of the mitochondrial bc1 cytochrome complex²² (Cbp3, PFAM: PF03981.16; HHpred probability 91%). In bacteria, however, the JukA functions were previously unknown. Proteins from the JukA family align with Cbp3 throughout their length except for a small N-terminal domain identified in Pfam as DUF3944 (PF13099). JukB has no clearly predicted molecular function.

JukA is much more widely spread than JukB, being present in 5,300 genomes (21%) compared with 262 genomes (1%) that encode JukB (Table S1). However, the distribution of these genes is strongly biased. JukA was mostly found in Pseudomonadota (previously known as Proteobacteria) (5,147 out of 14,098 genomes) and Cyanobacteriota (126 out of 194). Within Pseudomonadota, JukA homologs are most prominently enriched in Enterobacterales (4,450 out of 5,799), Campylobacterales (311 out of 760), Pseudomonadales (216 out of 962), and Aeromonadales (20 out of 168). JukB largely follows the same taxonomic distribution but was also identified in several Actinomycetota (16 out of 2,424) that lack JukA. Among the genomes from the Pseudomonas genus (888 altogether), JukA is present in 212 (23%) and JukB in 87 (10%), of which 85 genomes encode both JukA and JukB. Compared with other defense systems recently analyzed in a comparable number of genomes,^{23,24} JukA has a distinct distribution, being mostly represented in Pseudomonadota and

(D and E) Growth curves measuring OD600 during ϕ KZ infection in (D) PA14 and indicated mutants or (E) PAO1 and strains heterologously expressing *jukA* and *jukB* via either plasmid (*+pjukAB*) or chromosome integration (*::jukAB*), both from *jukAB* native promoter. Error bars in (D) and (E) represent one standard deviation calculated from two technical replicates.

(F) Spot titration (10 fold serial dilutions) of indicated phage on indicated bacterial lawns.

See also Figures S1 and S2.

Cyanobacteriota. In terms of representation among bacteria, JukA is relatively common, taking the third place after restriction-modification systems (present in 83% of the genomes) and CRISPR (39%), and more widely spread than Gabija, Wadjet, Retrons, CBASS, AbiE11, and Abi2 for which representation ranges from 10% to 17%.

Generally, the tree topology of JukA (Figure S6A) poorly reflects the taxonomy affiliation of respective genomes, at least on the genus level, which is consistent with horizontal gene transfer (HGT) playing considerable role in the evolution of this system. However, deep branching in the JukA phylogeny is consistent with higher level of bacterial taxonomy, so that JukAs from Gammaproteobacteria, Cyanobacteria, and Bacteroides form separate clades in the tree, suggesting that HGT occurs mostly within these higher taxa. Within the genus *Pseudomonas* and other bacterial genera, the distribution of JukA is patchy (Table S1), which also points to roles of HGT and lineage-specific gene loss in the evolution of the Juk system. Furthermore, the gene neighborhoods of *jukA* are highly diverse (Table S2), as expected of defense systems that are generally encoded within defense islands and prone to gene shuffling. Based on examination of these neighborhoods, we do not observe any conserved links to a specific mobile genetic element (MGE). However, careful analysis of the microevolution of JukA or JukB requires a separate study.

With limited functional information available on JukA and JukB, we decided to first test if Juk functions via mechanisms similar to known bacterial immune systems. Specifically, we tested whether the Juk system affected phage adsorption, had nuclease activity, or triggered abortive infection. PA14 and PA14Δ*jukAB* showed similar phage adsorption kinetics, although adsorption to both strains was generally slow compared with PAO1 (Figure S1B). Because this slow phage adsorption hinders plaqueing and microscopy assays, for the rest of the study, to study the mechanism of Juk immunity, we used PAO1 (Juk⁻) and PAO1::*jukAB* (Juk⁺) in which *jukAB* expression is driven from the chromosome by its native promoter. JukA and JukB showed no sequence or structural similarity to any known nucleases, and moreover, the multiple alignments of both families did not contain patterns of conserved charged or polar residues that could potentially form unknown nuclease active sites, suggesting that Juk is unlikely to directly cleave the ϕ KZ genome (Data S1). As shown by growth curves above, cells proliferate well, even at high MOIs, when armed with high levels of Juk. Additionally, fluorescence microscopy at high MOIs revealed infected cells that manifested Juk immunity continued cell division, with no cell death or dormancy observed (Figure S2B), indicating that Juk does not cause abortive infection, nor does it allow expression of phage genes that prevent growth.

Juk blocks the early stage of ϕ KZ infection

Using fluorescence microscopy, we followed the infection cycle of ϕ KZ to identify the stage of infection targeted by Juk. Around 50 min post-infection at MOI 1, Juk⁻ cells contained a mature ϕ KZ nucleus, whereas in Juk⁺ cells, the nucleus formation was completely abolished (Figure 2A). Prior to nucleus formation, the ejected ϕ KZ genome is enclosed in the EPI vesicle and pre-

sent as DAPI-stained puncta.^{7,10} The ejected genome was visible in 60% ($n = 306$ cells) of Juk⁻ cells but only in 14% ($n = 284$ cells) of Juk⁺ cells (Figure 2B), suggesting that the genome can enter the Juk⁺ cell but then is eliminated despite initially being enclosed in the EPI vesicle. Time-lapse imaging also showed the disappearance of the ϕ KZ genome in Juk⁺ cells (Figure S2C).

To corroborate the microscopy observations, we measured phage gDNA levels at two distal loci (*kz054* and *kz241*) by quantitative PCR (qPCR). *kz054* encodes chimallin, the major protein of the phage nucleus.^{12,13} Note that since MOIs <5 do not lead to successful ϕ KZ infection in Juk⁺ cells, we consider that all MOIs <5 have a similar effect on ϕ KZ infection cycle in Juk⁺ cells. Upon infection at MOI 0.5, ϕ KZ gDNA level initially increased in both Juk⁻ and Juk⁺ cells from 0 to 5 min, likely due to asynchronous phage entry (Figure 2C). After 5 min, ϕ KZ DNA level remained stable in Juk⁻ cells prior to phage DNA replication around 15 min, but it decreased in Juk⁺ cells (Figure 2C). The decay of ϕ KZ gDNA in Juk⁺ strain (~10-fold from 5 to 55 min, Figure 2C) was much faster than cell division (~30 min per division), suggesting the phage DNA is degraded. By contrast, at MOI 20, which is high enough to overwhelm Juk immunity, ϕ KZ gDNA level did not decrease after initial gDNA ejection in Juk⁺ cells (Figure S2D).

During infection, ejected ϕ KZ RNA polymerase (RNAP) immediately starts transcription of early ϕ KZ genes within the EPI vesicle.^{9,10,25} To confirm the action of Juk on the early stages of ϕ KZ infection, we quantified the expression levels of two early genes, *kz054* and *kz241*; one middle gene, *kz180*; and one late gene, *kz153*.²⁵ During low MOI infection of Juk⁺ cells, where Juk neutralizes ϕ KZ infection, a low level of early gene expression (*kz054* and *kz241*) was detected with no further increase in the amount of transcripts, while middle (*kz180*) and late (*kz153*) gene expression was not detected (Figure 2D). By contrast, in infected Juk⁻ cells, the amount of the transcripts of early genes *kz054* and *kz241* increased ~100- and 20-fold, respectively, by 15 min post-infection, and the transcripts of *kz180* and *kz153* were detected and started to increase around 15 min post-infection (Figure 2D). At MOI 20, where ϕ KZ overwhelms Juk immunity and completes its infection cycle, Juk immunity dramatically delayed increasing transcript levels but did not abolish expression (Figure S2E). Even at MOI 20, we did not observe a significant induction of *jukA* or *jukB* transcripts after phage infection, suggesting that expression of *juk* genes is not affected by ϕ KZ infection (Figure S2F). To gather a phage genome-wide view of transcription during Juk targeting of the phage, we also conducted whole-transcriptome profiling of ϕ KZ at MOIs that lead to failed or successful infections in Juk⁺ cells (Figure S3). This experiment similarly revealed a general abolition of early phage transcription across the genome, consistent with presented RT-qPCR of selected genes.

Lastly, we used proteomics to measure the effect of Juk immunity on the phage protein level at 5 min post- ϕ KZ infection (Figure 2E). MOI 2.5 was used to increase the number of ϕ KZ peptides for detection without overwhelming the Juk immune system. Early synthesized ϕ KZ proteins and ϕ KZ virion proteins were detected in infected Juk⁺ and Juk⁻ cells. The level of ejected phage virion protein gp093²⁶ remained similar between the Juk⁻ and Juk⁺ strains; however, early synthesized ϕ KZ

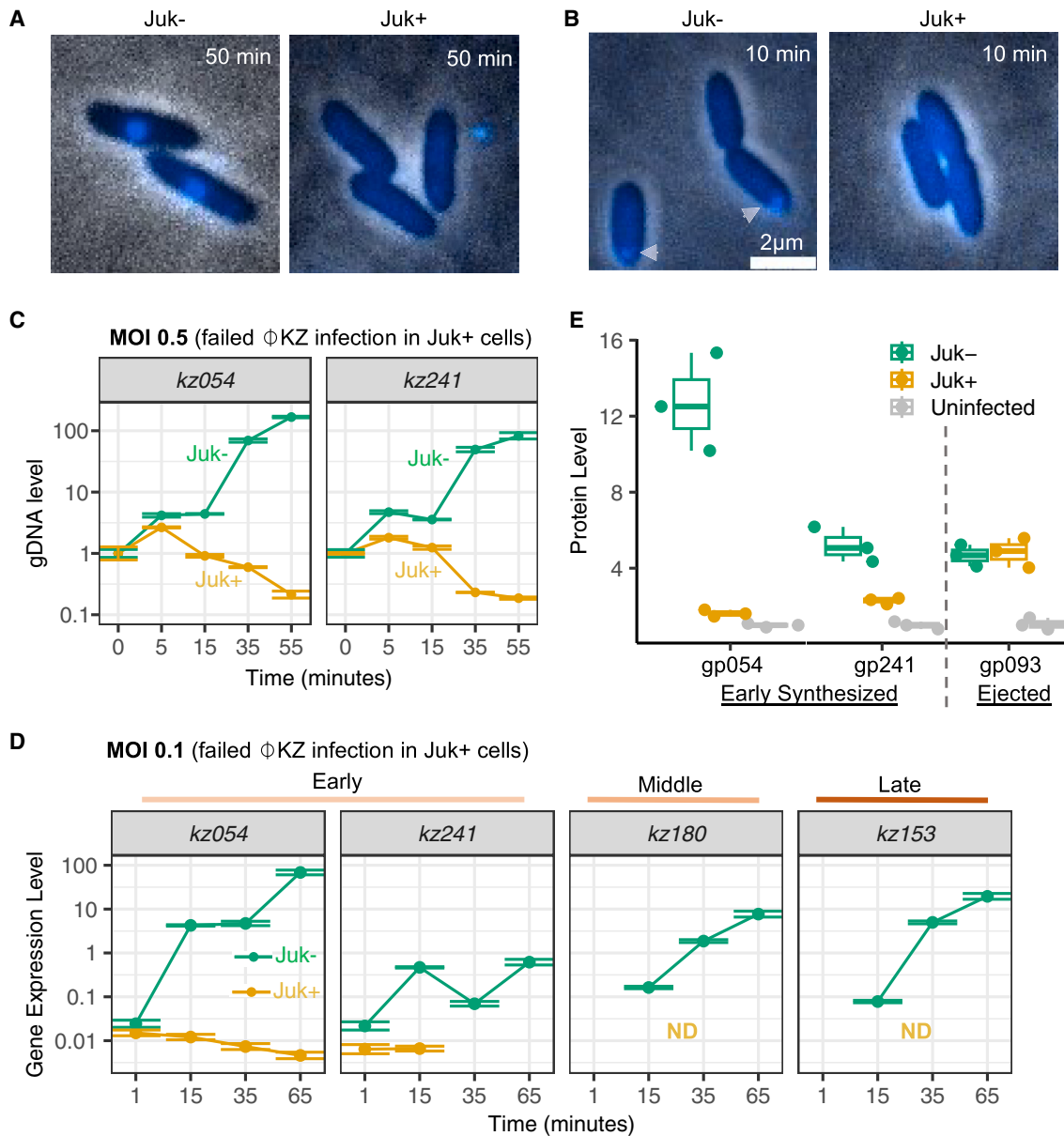


Figure 2. Juk immune system acts on early ϕ KZ infection

(A and B) ϕ KZ infection of indicated PAO1 cells with DAPI staining at (A) 50 or (B) 10 min post infection. Bacterial cells and ϕ KZ were incubated at 30°C for 10 min prior to imaging. Ejected ϕ KZ genomes are stained by DAPI and marked by arrows.

(C and D) (C) Quantification of the DNA level of two ϕ KZ genes over the course of infection at MOI 0.5. (D) Transcription level of ϕ KZ early (*kz054* and *kz241*), middle (*kz180*), and late (*kz153*) genes at MOI 0.1. Points below the assay detection limit were eliminated. “ND” indicates that the transcripts were not detected above the detection limit. Error bars in (C) and (D) represent one standard deviation calculated from two technical replicates.

(E) The level of phage proteins in ϕ KZ infected Juk⁻ and Juk⁺ cells and uninfected cells. The protein level was calculated by normalizing ϕ KZ protein intensity against the uninfected cells. Each dot represents one technical replicate. Cells were infected by ϕ KZ at MOI 2.5 and collected 5 min post infection. See also Figures S2 and S3.

proteins gp054 and gp241 were 8- and 2-fold lower in Juk⁺ strains than those in Juk⁻ strains, respectively. Together, these findings suggest that Juk immune proteins act rapidly to block essential early events of the phage life cycle occurring at the EPI vesicle, leading to ϕ KZ DNA degradation, likely through exposure to host nucleases.

JukA is the infection sensor in the two-component Juk immune system

To examine how Juk immunity detects ϕ KZ infection, we fluorescently tagged JukA and JukB (PAO1:: *mCherry-jukA/jukB-mNeonGreen*) and followed their localization. Fluorescent fusion did not affect Juk immunity (Figure S1D). Without ϕ KZ infection,

JukA was diffused in the cytoplasm whereas JukB presented as motile puncta (Figure 3A). However, upon ϕ KZ infection, JukA and JukB rapidly clustered at cell poles where the phage EPI vesicle is formed (Figure 3B). Related ϕ KZ-like phages ϕ PA3 and omko1 also induced JukA polar localization, whereas small dsDNA phages DMS3 and JBD30, which also infect at the cell pole,^{27,28} did not (Figure S2G). As discussed above, the ejected ϕ KZ genome is often rapidly cleared in Juk+ cells, but in those few cells where a DAPI-stained puncta (that is, ejected phage DNA) could be visualized, JukAB co-localized with it (zoom 2 in Figure 3B). To identify the driver of this polar localization phenotype, each Juk protein was expressed alone, showing that JukA sensed the infection on its own and localized to the infection site (Figure 3C), whereas JukB puncta formation and localization were entirely JukA dependent (Figure 3D). Because JukA by itself is not sufficient to abrogate infection, the co-localization of JukA puncta and the ejected ϕ KZ DNA were more apparent in the absence of JukB (Figure 3C). In the absence of JukB, JukA is recruited to the infected cell pole and then migrates adjacent to the maturing phage nucleus (Figure 3E). These findings suggest that JukA serves as a sensor of ϕ KZ infection by binding to phage factors at the EPI vesicle, which then recruits the putative effector JukB and together antagonize DNA protection and early transcription, two events executed by the EPI vesicle.

Phage protein gp241 is sufficient to recruit Juk and induce JukA and JukB binding

To determine which phage factor(s) triggers the JukA response, we searched for phage escape mutants, but none were successfully isolated. We therefore used a genomic screen with a plasmid library harboring random, sheared ϕ KZ gDNA fragments (~3 kb/fragment). Overexpression of factors from a multi-copy plasmid that induce the JukA response would potentially saturate JukA and partially or completely inhibit the Juk immunity. Growth curves of ~500 colonies of Juk+ cells expressing random ϕ KZ genes (5–6 \times ϕ KZ genome coverage) were measured with ϕ KZ infection. We identified four plasmids carrying ϕ KZ genes that partially rescued ϕ KZ infection in the presence of Juk (Figure S4A). While one plasmid carried a ϕ KZ gDNA fragment >80 kb, the other three (B1, C1, and F1) carried distinct but overlapping gDNA fragments ranging from 1.5 to 3 kb (Figure 4A). The gDNA inserts of B1, C1, and F1 mapped to a similar location in the phage genome with an overlap of two genes, *kz241* and *kz242* (Figure 4A). Both *kz241* and *kz242* are early genes transcribed from distinct ϕ KZ early promoters.²⁵

Strains carrying plasmids B1, C1, or F1 induced the localization of both Juk proteins to the cellular pole in the absence of ϕ KZ infection, phenocopying Juk localization in infected cells (Figures 4B and S4B). Removal of *kz241* from the C1 and F1 plasmids abolished Juk recruitment (Figures 4B and S4B), and a construct with *kz241* alone was sufficient to recruit Juk proteins (indicated by arrows in Figure 4C). Co-expression of gp241 and gp242 enhanced the recruitment of Juk proteins to the cellular pole, compared with that of gp241 alone; however, expression of gp242 alone did not recruit Juk proteins (Figure 4C). Fluorescence tagging of gp241 (gp241-mNeonGreen) expressed from a plasmid in uninfected cells showed that gp241 co-localized with JukA (mCherry-JukA) at the cellular pole (Figure 4D). gp241 has no known function but

is an early expressed protein predicted to be a membrane protein containing an N-terminal transmembrane (TMD) (4–23 aa) by TMHMM.²⁹ Removal of the TMD (Δ 2–23 aa) of gp241 abolished localization of gp241 and JukA to the cellular pole (Figure 4E).

Based on the above data, we sought to determine whether gp241 interacts with Juk proteins directly. We purified gp241 (12.9 kDa), JukA (27.7 kDa), and JukB (35.3 kDa) proteins and tested their interactions using an *in vitro* pull-down assay. JukA-containing His tag on its C terminus (JukA-His) was used as the bait. On SDS-PAGE, we noticed that in addition to the monomer band, JukB formed SDS-resistant high molecular weight oligomers at a molecular weight equivalent to JukB dimer, trimer, and tetramer (lane 2 in Figure 4F). Using mass spectrometry, we confirmed that these high molecular weight bands are indeed formed by JukB proteins (Figure S4C). Whereas JukB showed almost no binding to JukA-His in the assay (lane 9), gp241 not only bound directly to JukA-His (lane 8) but also substantially enhanced JukB pull-down by JukA-His (lane 10) (Figure 4F). Interestingly, removal of the TMD of gp241 neither affects its interaction with JukA proteins nor its ability to stimulate JukB binding (Figure S4D). This suggests the interaction with JukA is mediated via the cytoplasmic domain of gp241, but the cellular localization requires its TM region. We further measured the protein binding kinetics using surface plasmon resonance (SPR). We observed a binding K_D of 0.162 μ M between JukA and gp241 and a K_D of 31.6 μ M between JukA and JukB (Figure S4E), confirming the strong interaction between JukA and gp241 and the weak binding between JukA and JukB (Figure 4F). Additionally, a binding K_D of 20.6 μ M was observed between JukB and gp241, suggesting a weak interaction too (Figure S4E). Taken together, the soluble region of gp241, an early-expressed phage protein of unknown function, which is still produced at reduced levels in the presence of Juk (Figure 2E), is sufficient to directly bind JukA and enhance JukB binding *in vitro*.

JukB forms a tetramer with structural similarity to a pore-forming toxin

To explore the mechanisms by which JukB effector abolished phage infection, we solved its structure at a resolution of 2.44 Å by X-ray crystallography (Table S3). Four JukB homologs were attempted for protein crystallization, out of which only one JukB homolog from *Shewanella xiamenensis* (17.2% identity and 30.0% similarity to JukB from PA14, 35.8 kDa) was successfully crystallized and its structure determined. We named *jukA*-containing operons that offer immune function against ϕ KZ after their species name hereafter. For instance, the Juk system from *Shewanella xiamenensis* is named SxJuk, and the original Juk system from the *P. aeruginosa* strain PA14 is named PaJuk. SxJuk behaved similarly to the PaJuk immune system. For instance, both SxJukA and SxJukB are required for immunity against ϕ KZ infection (Figure S5A), and both proteins are recruited to the infection site at the pole (Figure S5B). Like PaJuk, SxJuk is also a non-abortive immune system as ϕ KZ-infected cells continue to divide rather than undergo programmed cell death or enter cell dormancy (Figure S5C).

In the solved structure, SxJukB forms a tetramer with a negatively charged pore in the middle (Figures 5A–5C). Size exclusion chromatography with multi-angle light scattering (SEC-MALS)

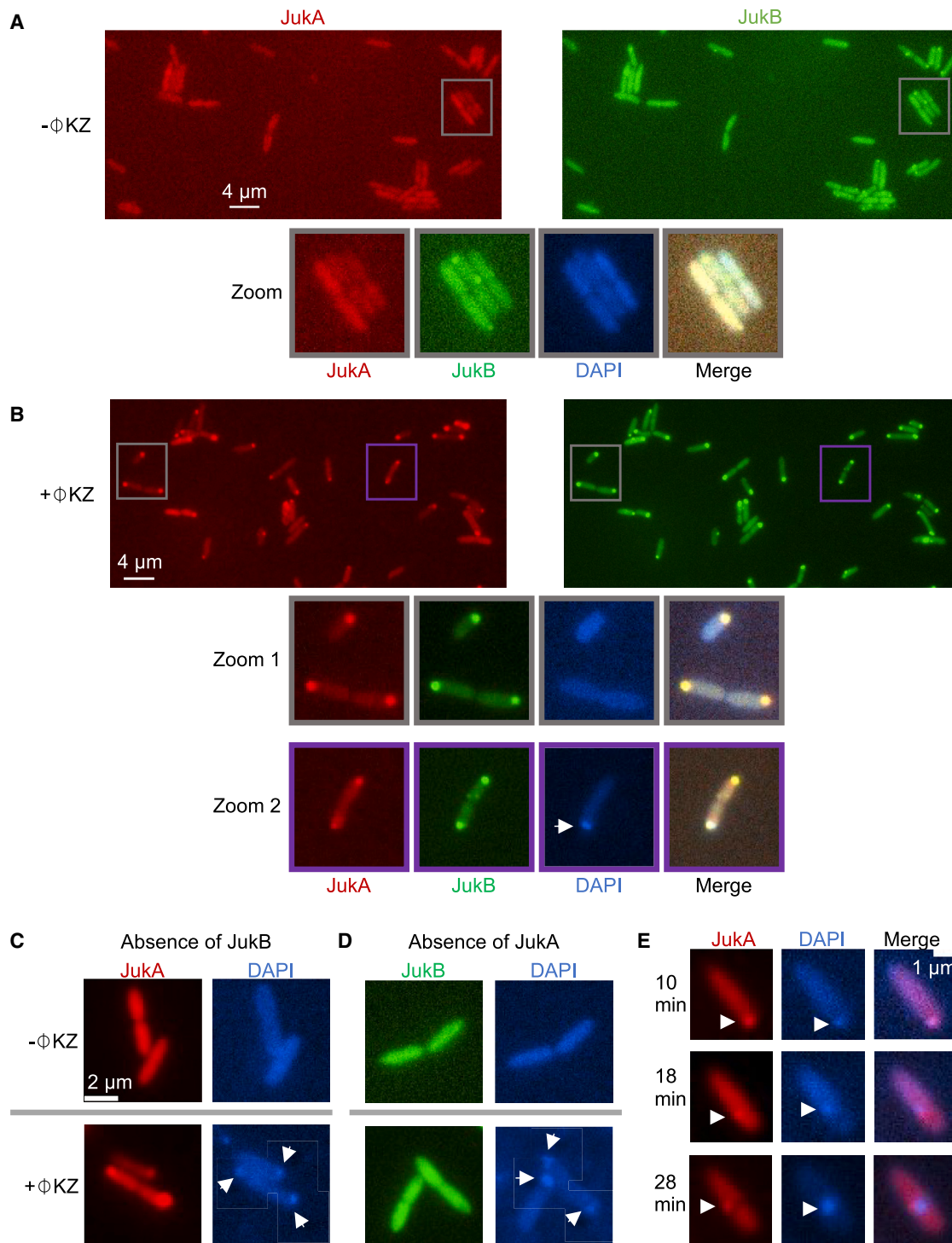


Figure 3. JukA is the infection sensor in the two component Juk immune system

(A–D) Fluorescence microscopy of JukA and JukB localization (A) without and (B) with ϕKZ infection in PAO1::mCherry *jukA/jukB* mNeonGreen strain. (C) JukA localization in the absence of JukB, using PAO1[pBAD::mCherry *jukA*] strain. (D) JukB localization in the absence of JukA, using PAO1[pBAD::jukB mNeonGreen] strain. In (A) (D), DAPI stained DNA are shown. Ejected ϕKZ genomes are marked by arrows. The scale is the same in (C) and (D).

(E) Time series visualization of JukA and phage genomes, using PAO1[pBAD::mCherry *jukA*] strain infected by ϕKZ . JukA puncta and ϕKZ genomes are indicated by arrows. Note that MOI 1 is used for ϕKZ infection. Infected cells are incubated at 30°C for 10 min before being subject to microscopy.

See also Figures S1 and S2.

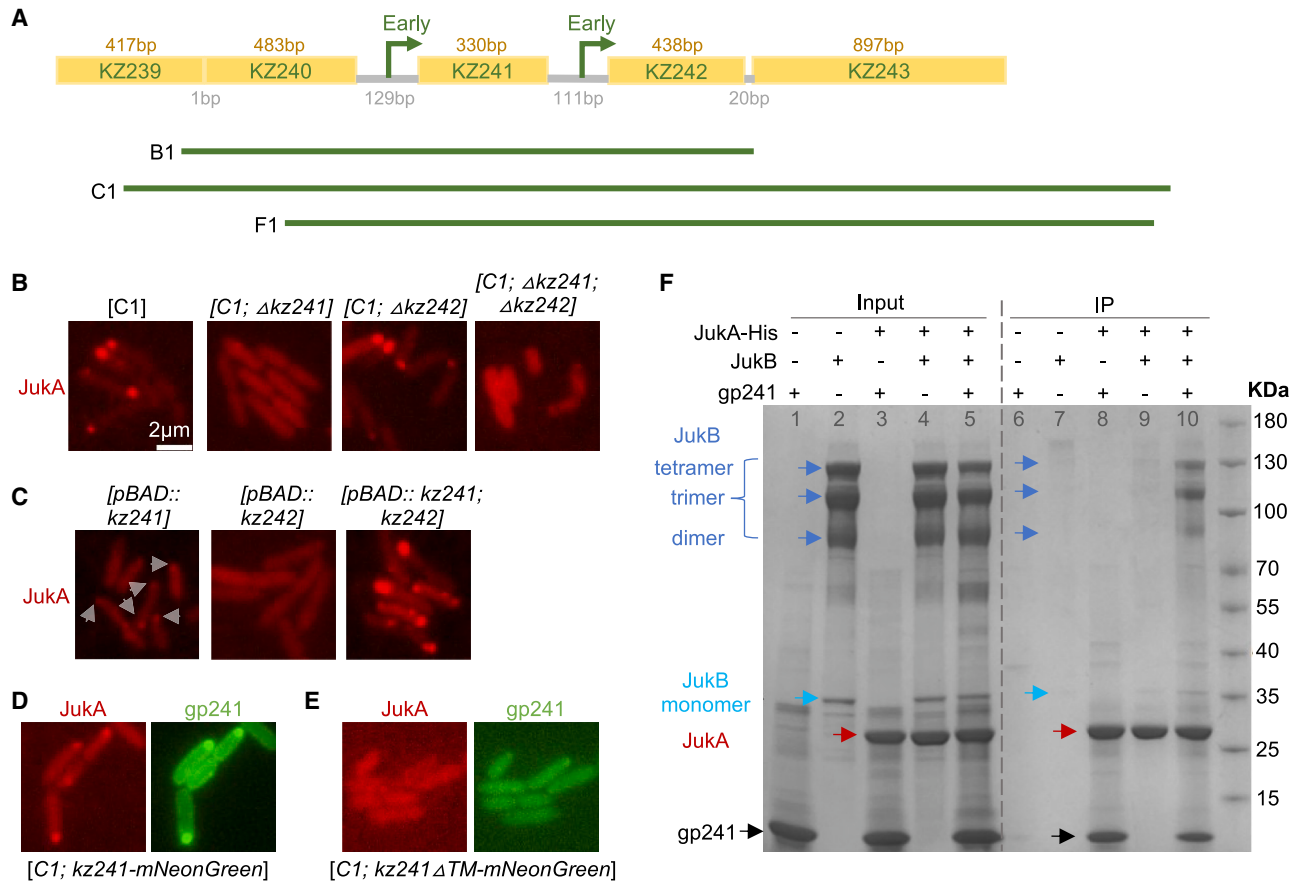


Figure 4. Phage protein gp241 is sufficient to recruit Juk proteins and to induce JukA and JukB binding

(A–C) (A) Map of ϕ KZ gDNA fragments carried by plasmids (B1, C1, and F1) that weaken Juk immunity. (B and C) In the absence of ϕ KZ infection, JukA and JukB localization in PAO1::mCherry *jukA/jukB* mNeonGreen strains carrying (B) wild type C1 plasmid or C1 plasmid with *kz241*, *kz242*, or *kz241+kz242* deleted, and (C) plasmids with *kz241*, *kz242*, or *kz241+kz242* under pBAD promoter induced by 0.25% arabinose. Weak JukA puncta at the cellular pole, which are induced by gp241 alone, are indicated by arrows. (D and E) In the absence of ϕ KZ infection, JukA and gp241 localization in PAO1::mCherry *jukA/jukB* strains carrying C1 plasmid with (D) gp241 being tagged by mNeonGreen on its C terminus and (E) the transmembrane domain (TMD) of gp241 deleted. Scale bars in (C) (E) are the same as in (B). (F) Coomassie stained SDS PAGE gel showing *in vitro* immunoprecipitation (IP) assays among purified proteins JukA, JukB, and gp241. JukA contains His tag on its C terminus and is used as the bait protein. + and - indicate the presence/absence of corresponding protein. Lanes 1–5 are input samples. Lanes 6–10 are IP samples. See also Figure S4.

assay also confirmed its tetrameric assembly (Figure S5D). Notably, SxJukB yields the best structural alignment with domain I of the pore-forming protein Cry3a that is produced and secreted by the soil bacterium *Bacillus thuringiensis*, with a root-mean-square deviation (RMSD) of ~ 3.3 Å and a Z score of 10.6, as revealed by Dali search server³⁰ (Figures 5D, 5E, and S5E). Based on the recent discovery of the transcriptionally active EPI vesicle at the start of the infection,^{9–11} we next wondered if JukB disrupts this structure.

The membrane of the EPI vesicle is thought to derive from the inner membrane of the bacterial host cell.^{10,11} We made lipid-bilayer liposomes with phosphatidylethanolamine (PE), the dominant component of the inner membrane of *P. aeruginosa*, and tested whether purified PaJukA and PaJukB proteins disrupted these liposomes *in vitro*. The liposomes were filled with self-quenched fluorescent dye calcein, which does not fluoresce when at high concentrations. When liposomes are permeabilized, calcein

released from liposomes becomes fluorescent (Figure 5F). We conducted assays with PaJukA and PaJukB at low concentrations (1.2 nM) that minimally perturbed liposomes on their own, compared with the PBS control (Figures 5G and S5F). PaJukA together with PaJukB permeabilized liposomes (Figure 5G), which was further enhanced by the addition of gp241 (1.2 nM) (JukA+JukB+gp241 in Figure 5G). This improved effect is potentially caused by gp241 strengthening the interaction between PaJukA and PaJukB (Figure 4F). Notably, mutation of the conserved residues of PaJukA (R73A/K74A) abolished liposome permeabilization activity (Figure 5H), *in vivo* recruitment of PaJukA to the cellular pole upon ϕ KZ infection (Figure S5G), and phage inhibition (Figure S5I). From these findings, we propose that PaJukA is recruited to the EPI vesicle, likely with the help of gp241, which then recruits the effector PaJukB to destabilize the EPI vesicle. Given the non-abortive activity of Juk, we propose that JukB functions by forming pores not in the bacterial inner membrane but in the membrane of

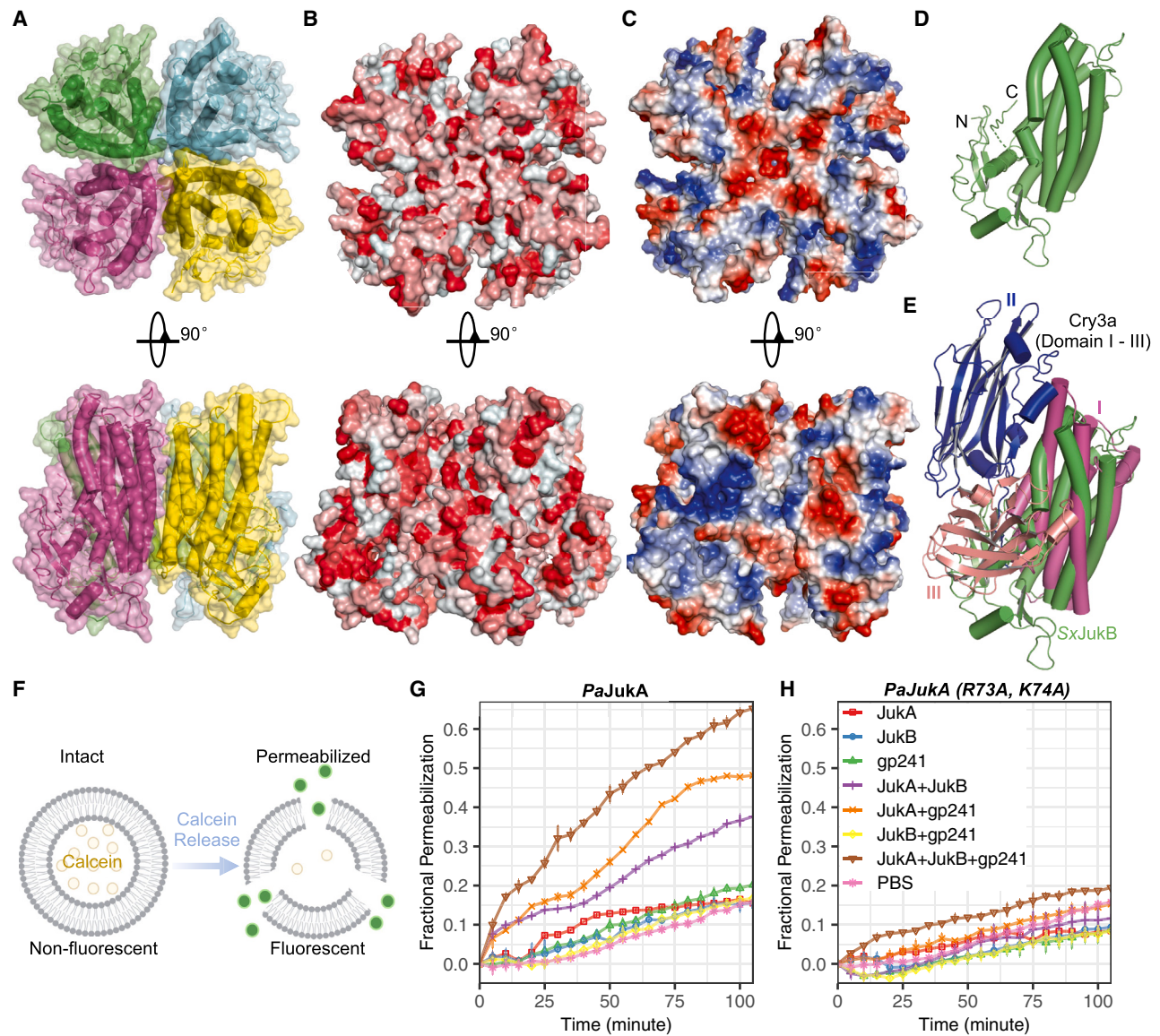


Figure 5. JukB tetramer structure resembles pore forming toxin

(A-C) (A) Structure of the tetramer form of SxJukB, (B) colored by the hydrophobicity (red: hydrophobic, white: hydrophilic), (C) colored by surface electrostatics (white: neutral, blue: positive, red: negative surfaces).

(D and E) (D) Structure of SxJukB monomer and (E) structural alignment between SxJukB and Cry3a (PDB: 4QX2).

(F) Schematics of the liposome calcein assay.

(G and H) Fraction of liposomes that are permeabilized by purified proteins with PBS as the negative control. Purified proteins were at a final concentration of 1.2 nM. Wild type *PaJukA* was used in (G). (R73A,K74A) mutated *PaJukA* protein was used in (H). Error bars represent one standard deviation calculated from two technical replicates.

See also [Figure S5](#).

the EPI vesicle, disrupting early phage gene expression, arresting the infection, and subsequently exposing ϕ KZ gDNA to downstream degradation.

Juk systems encompass numerous, distinct putative effectors in diverse bacteria

Having uncovered JukA as a sensor protein, we next surveyed where it is found in bacteria and which putative effectors are en-

coded nearby. Many widely distributed homologs of JukA were identified with conserved amino acid residues (N66, S67, R73, K74, Y79, K89, and E104) across the family, which are required to block ϕ KZ replication in *P. aeruginosa* (Figures S5H and S5I). Gene context analysis of *jukA* genes revealed a strong link with various defense systems (Table S2). At least one previously characterized or predicted defense gene is present in 173 of 329 representative loci (Figure S6A). WYL domain

proteins^{31,32} and components of restriction-modification systems are most frequent defense-associated genes in *jukA* neighborhoods. Apart from *jukB* (46 out of 329 loci), genes of several other families are predicted to form operons and are likely co-expressed with *jukA*. In particular, these putative JukA partners include O-antigen ligase RfaL,³³ uncharacterized PD-(D/E)XK, uncharacterized HNH family nucleases with TMDs, Xre family transcriptional regulators, and several uncharacterized proteins like DUF2541 (PF10807) and EcsC-like (PF12787) (Figure 6A). Furthermore, JukA fusions to Ras-like GTPase, a putative phospholipase of α/β hydrolase superfamily, and a domain of unknown function containing a coiled-coil region were also identified (Figure 6A). Based on these observations, we hypothesize that JukA functions as a jumbo phage sensor that combines with various effectors.

To test the functions of these JukA-containing operons in a consistent background, 18 operons representing different parts of the JukA phylogenetic tree were synthesized and expressed in PAO1 that was infected with a panel of phages (Figure S6B). Of these 18 operons, 8 operons (from *Leclercia pneumoniae*, *Jinshanibacter zhutongyuii*, *Desulfolutivibrio sulfoxidireducens*, *Flammeovirga kamogawensis*, *Stenotrophomonas maltophilia*, *Rhodospirillum centenum*, *Shewanella xiamenensis*, and *Vibrio taketomensis*) contained *jukB* as the putative effector (Figure S6B). Six of the eight JukAB homologs blocked ϕ KZ replication (Figure S6C). Deletion of either *jukA* or *jukB* from the JzJuk, SmJuk, RcJuk, or SxJuk operons abolished the immune function, indicating that these distinct Juk variants are also two-component systems (Figures S5A and S6D).

Next, we assayed 10 predicted operons with diverse putative effectors (Figure S6B). Four operons from *Vibrio alginolyticus* (VaJuk), *Escherichia marmotae* (EmJuk), *Janthinobacterium svalbardensis* (JsJuk), and *Pseudomonas fluorescens* (PfJuk), provided specific immunity against ϕ KZ-related jumbo phages (Figure S6C). PfJuk consisted of a single fusion protein containing a putative phospholipase domain and the JukA domain. Single amino acid mutagenesis of the catalytic triad residues within the PfJuk phospholipase domain (S145A, D202A, and H240A)³⁴ abolished its immune function (Figure 6B), suggesting that PfJuk phospholipase activity is essential for PfJuk immunity. EmJukA and JsJukA were paired with Xre family transcription regulators, while VaJukA was paired with a protein containing a helix-turn-helix (HTH) domain. Deletion of either *jukA* or the putative partner gene showed that in all three cases, JukA alone was sufficient for immunity (Figure S6D). Although EmJukA, JsJukA, and VaJukA proteins appeared to provide immunity independent of any partner, these JukAs contain no identifiable additional domains. To test whether these putative JukA-only immune systems blocked ϕ KZ infection similarly to PaJuk, we tagged these JukAs with mCherry and observed the same subcellular distribution as the original PaJukA, namely, diffuse in uninfected cells but rapidly concentrating to the infection site upon phage infection (Figure 6C). However, unlike original Juk immunity, where the phage genome disappeared over time, these JukA proteins, in the absence of putative effectors, appeared to arrest ϕ KZ infection at an early stage without subsequent phage genome degradation (Figure S6E), suggesting a different immune mechanism without a separate effector. Together, we identified 10 additional

Juk immune systems that use JukA protein or JukA domain as the putative sensor. The existence of functional anti- ϕ KZ immunity in diverse bacteria suggests that these bacteria are hosts to ϕ KZ-like nucleus-forming jumbo phages and evolved mechanisms to inhibit a key early stage in the reproduction of these phages' life cycle in a non-abortive manner.

Lastly, having identified gp241 as an activator of Juk, we asked whether its deletion allowed for Juk evasion. We constructed a phage mutant by deleting *kz241* gene from the ϕ KZ genome and tested if the Δ *kz241* mutant escaped recognition by different Juk immune systems. Surprisingly, despite gp241 being sufficient for PaJuk activation, the Δ *kz241* mutant phage was efficiently targeted by PaJuk in plaque assays (Figure S6F) and still induced PaJukA recruitment to the cell pole (Figure S6G). Thus, ϕ KZ likely encodes a redundant trigger besides gp241 that induces PaJuk. Interestingly, we found that Δ *kz241* mutant plaqued \sim 100-fold better than the wild-type ϕ KZ when being targeted by the PfJuk immune system that harbors a diverged JukA fused to a predicted phospholipase domain (Figure 6D). Additional constructed phage mutants lacking *kz241* (Δ *kz236-241*, Δ *kz241-242*) also escaped PfJuk immunity whereas a Δ *kz237* control mutant did not (Figure 6D). Taken together, these findings demonstrate that Juk systems, including PaJuk and PfJuk, likely sense multiple redundant factors in addition to gp241. The ability of Juk to still limit phage replication when one *bone fide* trigger is removed highlights a versatile detection ability by Juk.

DISCUSSION

It has been recently established that phages in the ϕ KZ family build an EPI vesicle, an endosome-like structure that protects the phage DNA, where early phage genes are transcribed by an injected RNAP.⁷⁻¹¹ Here, we showed that JukA sensor protein binds directly to an early gene product (gp241) and localizes rapidly to the phage-infected pole where the EPI vesicle is located. The gp241 protein contains a TMD that is required for its localization to the cell pole but not for JukA binding. gp241 binding stimulates recruitment of the tetrameric JukB effector both *in vivo* and *in vitro*. When Juk is activated, the normal function of the EPI vesicle in early gene expression is interfered with and progression to the proteinaceous nucleus is halted. The PfJuk immune system consists of a single fusion protein containing JukA and phospholipase domains, suggesting that effectors accompanying the JukA sensor use different strategies to destabilize the EPI vesicle of ϕ KZ-like phages. Juk systems that only consist of a JukA do not appear to induce phage genome degradation and likely bind the EPI vesicle and arrest progression to the phage nucleus without destabilizing the vesicle. Unlike the orphan JukA systems, JukA alone from the JukAB systems does not offer immune function. Since all Juk systems were tested in the same host strain, this suggests that either the orphan JukA system interferes with the EPI vesicle on its own or is better at taking advantage of a host factor. The specificity of Juk systems in antagonizing ϕ KZ-like phages is likely determined by its ability to recognize specific phage factors and to target the EPI vesicle, which has not been reported in other phages. Phage factors besides gp241 that redundantly activate Juk remain to be discovered.

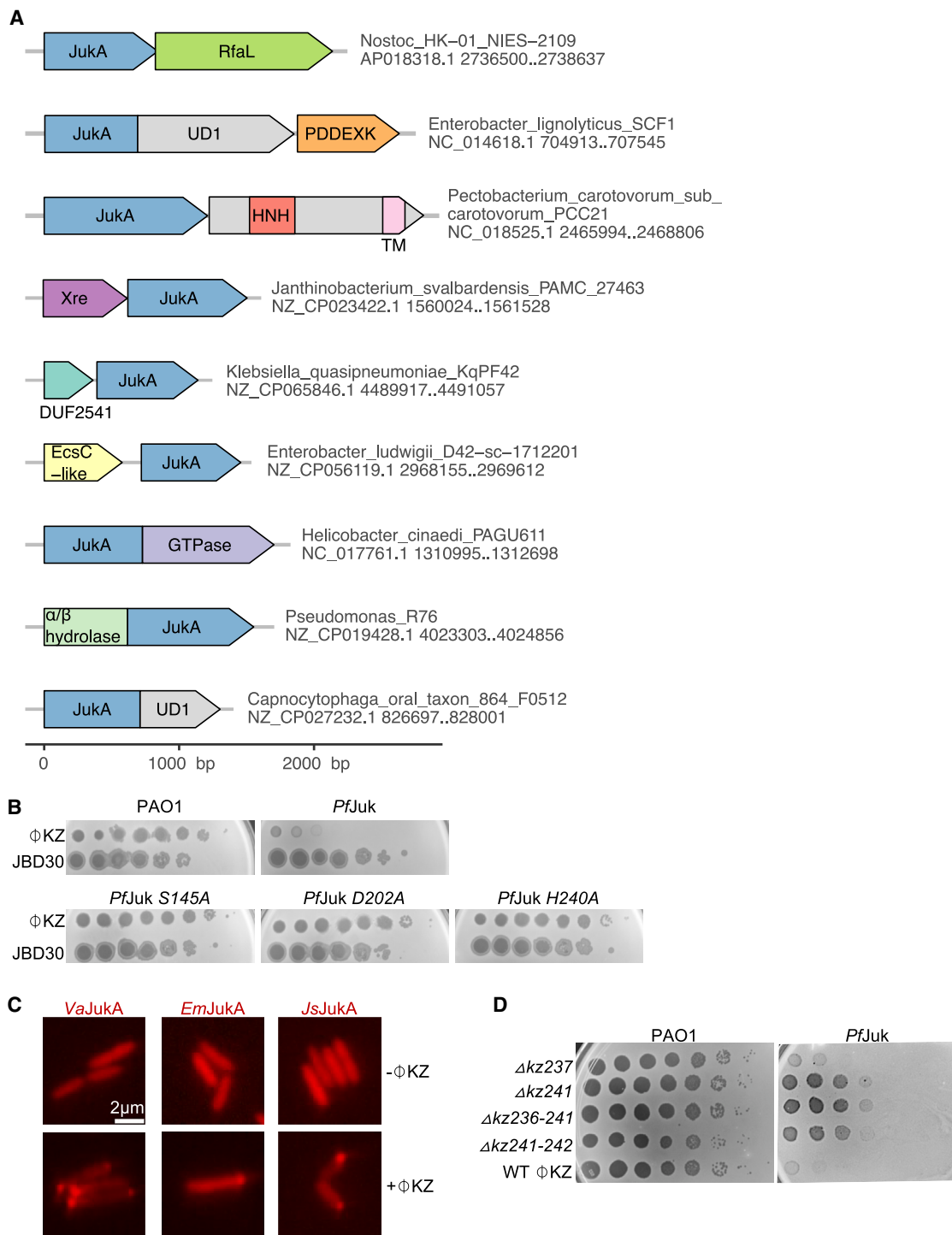


Figure 6. Jumbo phage killer systems encompass numerous, distinct putative effectors in diverse bacteria

(A) Organization of jukA neighborhoods. Genes are shown as arrows. Genes and untranslated regions are proportional for their sizes. The domain boundaries are approximate. Bacteria strain name, genome identifier, and the coordinates of depicted genes are shown on the right.

(B) Spot titration (10 fold serial dilutions) of ϕ KZ and the control phage JBD30 on the lawn of PAO1, PAO1 expressing wild type PflJuk, and PAO1 expressing mutated PflJuk.

(C) Localization of JukA homologs containing an N terminal mCherry tag in the absence and presence of ϕ KZ infection. MOI 1 is used for ϕ KZ infection.

(D) Spot titration (10 fold serial dilutions) of wild type ϕ KZ and its mutants on indicated bacterial lawns.

The expression of PflJuk and its mutants in (B) and (D) were induced by 0.2% arabinose.

See also Figure S6.

The non-abortive Juk mechanism acting quickly and directly on the phage is notable for a few reasons. First, detecting a phage protein and activating a direct anti-phage response, as opposed to acting on the cell to induce death or dormancy, is an emergent anti-phage mechanism. Second, the ability of JukB and the distinct phospholipase effector to act not on the bacterial inner membrane but on a lipid-containing phage structure represents a distinct target for immune effectors. Third, while this mechanism ensures cell survival, an apparent downside of this strategy is that high MOI infections can bypass Juk, likely because not all EPI vesicles can be effectively antagonized. The widespread identification of Juk proteins across diverse bacterial species suggests that nucleus-forming jumbo phages are more common than presently appreciated.

Limitations of the study

Here, we describe Juk, a defense system that targets the EPI vesicle and antagonizes early gene transcription, thus blocking downstream phage replication and nucleus formation. The EPI vesicle is the site of early gene transcription via injected RNAP.^{9–11} Using Cas13 proteins to bind to the early mRNA encoding chimallin (the major nucleus protein) and block translation in ϕ KZ⁵ or *E. coli* phage Goslar⁹ indeed blocks nucleus assembly but does not lead to phage genome degradation. Instead, the phage genome remains stable, presumably within the EPI vesicle. Thus, we presume that EPI vesicle disruption or lysis by PaJuk is required to expose the phage genome to nucleases in the cytoplasm, explaining the clearance of phage DNA. However, those nucleases do not appear to be a core part of the Juk system, thus they have not been identified here and remain speculative. In this study, we demonstrated the role of the JukA-JukB-gp241 complex in disrupting liposomes *in vitro*. However, *in situ* structural characterization (i.e., cryo-ET) of this complex is required to understand how it interacts with and disrupts the ϕ KZ EPI vesicle. Additionally, further studies are needed to identify the additional phage factors that activate the Juk systems as ϕ KZ mutants lacking gp241 still activated Juk. Lastly, many diverse Juk systems are present in bacteria that do not have known ϕ KZ-like phages, and thus we were limited to testing the effects of stand-alone JukA proteins and various JukA-adjacent effectors in *P. aeruginosa*. Some systems provided robust anti- ϕ KZ immunity, but not all systems induced phage genome degradation. These data suggest that phage genome degradation is not a requirement for Juk function, but this would best be assayed in native hosts with cognate phages.

RESOURCE AVAILABILITY

Lead contact

Requests for resources will be fulfilled by the lead contact, Joseph Bondy Denomy (joseph.bondy_denomy@ucsf.edu).

Materials availability

Materials generated in this paper are listed in the [key resources table](#) and available from the [lead contact](#).

Data and code availability

Protein structure data are deposited at Protein Data Bank (PDB: 9JHT). Proteomics data are deposited into the PRIDE database (PRIDE: PXD052338).

ACKNOWLEDGMENTS

This work in the Bondy Denomy lab was supported by the National Institutes of Health (NIH) (R01AI171041 01) and the UCSF Program for Breakthrough Biomedical Research funded in part by the Sandler Foundation. K.S.M. and E.V.K. are funded through the Intramural Research Program of NIH (National Library of Medicine). D.A. is funded by the NIH (R35GM118099). Y.F. is funded by the National Key Research and Development Program of China (2022YFC3401500 and 2022YFC2104800). We thank Dr. Stephen Lory for sharing materials used to construct the Tn mutant library and Dr. Michael Boucher for sharing expertise on Tn genomic library construction. We thank Dr. Andrea Fossati and Bondy Denomy lab members for their constructive comments.

AUTHOR CONTRIBUTIONS

L.Y. conceived the project, designed and performed experiments, and wrote the manuscript. L.G., S.Y., and X.C. performed protein purification, crystallization, data collection, and biochemical assays, designed and supervised by Y.F. Y.F. solved the structure of SxJukB. I.B. and F.S. performed proteomics, supervised by M.S. and A.T. S.H., J.G., and D.A. contributed to execution of experiments, phage mutant construction, and experimental design, respectively. A.B., K.L., and K.R. optimized protein purification. K.S.M. and E.V.K. performed the bioinformatic analysis. J.B. D. supervised the project, designed experiments, and wrote the manuscript.

DECLARATION OF INTERESTS

J.B. D. is a scientific advisory board member of SNIPR Biome, Excision Bio therapeutics, LeapFrog Bio, and Acrigen Biosciences and is a co founder of Acrigen Biosciences and ePhective Therapeutics. The Bondy Denomy lab received research support from Felix Biotechnology.

STAR★METHODS

Detailed methods are provided in the online version of this paper and include the following:

- [KEY RESOURCES TABLE](#)
- [EXPERIMENTAL MODEL AND STUDY PARTICIPANT DETAILS](#)
 - *Pseudomonas aeruginosa* strains
 - Bacterial strains for protein purification
 - Bacteriophages
- [METHOD DETAILS](#)
 - Bacterial transformation
 - Genetic manipulation
 - Phage plaque assays
 - Growth curve experiments
 - PA14 Transposon mutant library Screening
 - Adsorption assay
 - Fluorescence microscopy and imaging
 - qPCR and RT qPCR
 - RNA sequencing
 - JukA and JukB mutagenesis
 - ϕ KZ gDNA plasmid library construction
 - Screening phage factors inducing Juk response
 - Whole proteomics assay
 - ϕ KZ genetic editing
 - Protein expression and purification
 - In vitro pull down assay
 - Surface Plasmon Resonance binding assay
 - Protein crystallization
 - Data collection and structure determination
 - Liposome Calcein leakage assay
 - Selecting *jukA* containing operons for testing
 - Multiple sequence alignment of Juk proteins
 - Analysis of JukA and JukB distribution
- [QUANTIFICATION AND STATISTICAL ANALYSIS](#)

SUPPLEMENTAL INFORMATION

Supplemental information can be found online at <https://doi.org/10.1016/j.cell.2025.02.016>.

Received: October 1, 2024

Revised: December 24, 2024

Accepted: February 20, 2025

Published: March 19, 2025

REFERENCES

1. Millman, A., Bernheim, A., Stokar Avihail, A., Fedorenko, T., Voicheck, M., Leavitt, A., Oppenheimer Shaanan, Y., and Sorek, R. (2020). Bacterial Retrons Function In Anti Phage Defense. *Cell* 183, 1551–1561.e12. <https://doi.org/10.1016/j.cell.2020.09.065>.
2. Lopatina, A., Tal, N., and Sorek, R. (2020). Abortive Infection: Bacterial Suicide as an Antiviral Immune Strategy. *Annu. Rev. Virol.* 7, 371–384. <https://doi.org/10.1146/annurev-virology-011620-040628>.
3. Bernheim, A., and Sorek, R. (2020). The pan immune system of bacteria: antiviral defence as a community resource. *Nat. Rev. Microbiol.* 18, 113–119. <https://doi.org/10.1038/s41579-019-0278-2>.
4. Koonin, E.V., Makarova, K.S., and Wolf, Y.I. (2017). Evolutionary Genomics of Defense Systems in Archaea and Bacteria. *Annu. Rev. Microbiol.* 71, 233–261. <https://doi.org/10.1146/annurev-micro-090816-093830>.
5. Mendoza, S.D., Nieweglowska, E.S., Govindarajan, S., Leon, L.M., Berry, J.D., Tiwari, A., Chaikerasitak, V., Pogliano, J., Agard, D.A., and Bondy Denomy, J. (2020). A bacteriophage nucleus like compartment shields DNA from CRISPR nucleases. *Nature* 577, 244–248. <https://doi.org/10.1038/s41586-019-1786-y>.
6. Malone, L.M., Warring, S.L., Jackson, S.A., Warnecke, C., Gardner, P.P., Gumy, L.F., and Fineran, P.C. (2020). A jumbo phage that forms a nucleus like structure evades CRISPR Cas DNA targeting but is vulnerable to type III RNA based immunity. *Nat. Microbiol.* 5, 48–55. <https://doi.org/10.1038/s41564-019-0612-5>.
7. Danilova, Y.A., Belousova, V.V., Moiseenko, A.V., Vishnyakov, I.E., Yakunina, M.V., and Sokolova, O.S. (2020). Maturation of Pseudo Nucleus Compartment in *P. aeruginosa*, Infected with Giant phiKZ Phage. *Viruses* 12, 1197. <https://doi.org/10.3390/v12101197>.
8. Laughlin, T.G., Deep, A., Prichard, A.M., Seitz, C., Gu, Y., Enustun, E., Suslov, S., Khanna, K., Birkholz, E.A., Armbruster, E., et al. (2022). Architecture and self assembly of the jumbo bacteriophage nuclear shell. *Nature* 608, 429–435. <https://doi.org/10.1038/s41586-022-05013-4>.
9. Armbruster, E.G., Lee, J., Hutchings, J., VanderWal, A.R., Enustun, E., Adler, B.A., Aindow, A., Deep, A., Rodriguez, Z.K., Morgan, C.J., et al. (2023). Sequential membrane and protein bound organelles compartmentalize genomes during phage infection. Preprint at bioRxiv. <https://doi.org/10.1101/2023.09.20.558163>.
10. Antonova, D., Nichiporenko, A., Sobinina, M., Wang, Y., Vishnyakov, I.E., Moiseenko, A., Kurdyumova, I., Chesnokov, Y.M., Stepanchikova, E., Bourkaltseva, M., et al. (2024). Genomic transfer via membrane vesicle: a strategy of giant phage phiKZ for early infection. *J. Virol.* 0, e00205 24. <https://doi.org/10.1128/jvi.00205-24>.
11. Mozumdar, D., Fossati, A., Stevenson, E., Guan, J., Nieweglowska, E., Rao, S., Agard, D., Swaney, D.L., and Bondy Denomy, J. (2024). Characterization of a lipid based jumbo phage compartment as a hub for early phage infection. *Cell Host Microbe* 32, 1050–1058.e7. <https://doi.org/10.1016/j.chom.2024.05.016>.
12. Chaikerasitak, V., Nguyen, K., Khanna, K., Brilot, A.F., Erb, M.L., Coker, J.K.C., Vavilina, A., Newton, G.L., Buschauer, R., Pogliano, K., et al. (2017). Assembly of a nucleus like structure during viral replication in bacteria. *Science* 355, 194–197. <https://doi.org/10.1126/science.aal2130>.
13. Chaikerasitak, V., Nguyen, K., Egan, M.E., Erb, M.L., Vavilina, A., and Pogliano, J. (2017). The phage nucleus and tubulin spindle are conserved among large *Pseudomonas* phages. *Cell Rep.* 20, 1563–1571. <https://doi.org/10.1016/j.celrep.2017.07.064>.
14. Mayo Muñoz, D., Smith, L.M., Garcia Doval, C., Malone, L.M., Harding, K.R., Jackson, S.A., Hampton, H.G., Fagerlund, R.D., Gumy, L.F., and Fineran, P.C. (2022). Type III CRISPR Cas provides resistance against nucleocleus forming jumbo phages via abortive infection. *Mol. Cell* 82, 4471–4486.e9. <https://doi.org/10.1016/j.molcel.2022.10.028>.
15. van Belkum, A., Soriaga, L.B., LaFave, M.C., Akella, S., Veyrieras, J. B., Barbu, E.M., Shortridge, D., Blanc, B., Hannum, G., Zambardi, G., et al. (2015). Phylogenetic Distribution of CRISPR Cas Systems in Antibiotic Resistant *Pseudomonas aeruginosa*. *mBio* 6, e01796 15. <https://doi.org/10.1128/mBio.01796-15>.
16. Makarova, K.S., Wolf, Y.I., Iranzo, J., Shmakov, S.A., Alkhnbashi, O.S., Brouns, S.J.J., Charpentier, E., Cheng, D., Haft, D.H., Horvath, P., et al. (2020). Evolutionary classification of CRISPR Cas systems: a burst of class 2 and derived variants. *Nat. Rev. Microbiol.* 18, 67–83. <https://doi.org/10.1038/s41579-019-0299-x>.
17. Kim, M.K., Chen, Q., Echterhof, A., McBride, R.C., Pennetzdorfer, N., Banaei, N., Burgener, E.B., Milla, C.E., and Bollyky, P.L. (2024). A Blueprint for Broadly Effective Bacteriophage Therapy Against Bacterial Infections. Preprint at bioRxiv. <https://doi.org/10.1101/2024.04.20.590411>.
18. Liberati, N.T., Urbach, J.M., Miyata, S., Lee, D.G., Drenkard, E., Wu, G., Villanueva, J., Wei, T., and Ausubel, F.M. (2006). An ordered, nonredundant library of *Pseudomonas aeruginosa* strain PA14 transposon insertion mutants. *Proc. Natl. Acad. Sci. USA* 103, 2833–2838. <https://doi.org/10.1073/pnas.0511100103>.
19. Chan, B.K., Siström, M., Wertz, J.E., Kortright, K.E., Narayan, D., and Turner, P.E. (2016). Phage selection restores antibiotic sensitivity in MDR *Pseudomonas aeruginosa*. *Sci. Rep.* 6, 26717. <https://doi.org/10.1038/srep26717>.
20. Danis Włodarczyk, K., Vandenheuevel, D., Jang, H.B., Briens, Y., Olszak, T., Arabski, M., Wasik, S., Drabik, M., Higgins, G., Tyrrell, J., et al. (2016). A proposed integrated approach for the preclinical evaluation of phage therapy in *Pseudomonas* infections. *Sci. Rep.* 6, 28115. <https://doi.org/10.1038/srep28115>.
21. Monson, R., Foulds, I., Foweraker, J., Welch, M., and Salmond, G.P.C. (2011). The *Pseudomonas aeruginosa* generalized transducing phage phiPA3 is a new member of the phiKZ like group of 'jumbo' phages, and infects model laboratory strains and clinical isolates from cystic fibrosis patients. *Microbiology* 157, 859–867. <https://doi.org/10.1099/mic.0.044701-0>.
22. Ndi, M., Masuyer, G., Dawitz, H., Carlström, A., Michel, M., Elofsson, A., Rapp, M., Stenmark, P., and Ott, M. (2019). Structural basis for the interaction of the chaperone Cbp3 with newly synthesized cytochrome b during mitochondrial respiratory chain assembly. *J. Biol. Chem.* 294, 16663–16671. <https://doi.org/10.1074/jbc.RA119.010483>.
23. Georjon, H., and Bernheim, A. (2023). The highly diverse antiphage defence systems of bacteria. *Nat. Rev. Microbiol.* 21, 686–700. <https://doi.org/10.1038/s41579-023-00934-x>.
24. Tesson, F., Hervé, A., Mordret, E., Touchon, M., d’Humières, C., Cury, J., and Bernheim, A. (2022). Systematic and quantitative view of the antiviral arsenal of prokaryotes. *Nat. Commun.* 13, 2561. <https://doi.org/10.1038/s41467-022-30269-9>.
25. Ceysens, P. J., Minakhin, L., Van den Bossche, A., Yakunina, M., Klimuk, E., Blasdel, B., De Smet, J., Noben, J. P., Bläsi, U., Severinov, K., et al. (2014). Development of Giant Bacteriophage phiKZ Is Independent of the Host Transcription Apparatus. *J. Virol.* 88, 10501–10510. <https://doi.org/10.1128/JVI.01347-14>.
26. Guan, J., Oromí Bosch, A., Mendoza, S.D., Karambelkar, S., Berry, J.D., and Bondy Denomy, J. (2022). Bacteriophage genome engineering with CRISPR Cas13a. *Nat. Microbiol.* 7, 1956–1966. <https://doi.org/10.1038/s41564-022-01243-4>.
27. Bondy Denomy, J., Qian, J., Westra, E.R., Buckling, A., Guttman, D.S., Davidson, A.R., and Maxwell, K.L. (2016). Prophages mediate defense

- against phage infection through diverse mechanisms. *ISME J.* 10, 2854–2866. <https://doi.org/10.1038/ismej.2016.79>.
28. Tsao, Y. F., Taylor, V.L., Kala, S., Bondy Denomy, J., Khan, A.N., Bona, D., Cattoir, V., Lory, S., Davidson, A.R., and Maxwell, K.L. (2018). Phage Morons Play an Important Role in *Pseudomonas aeruginosa* Phenotypes. *J. Bacteriol.* 200, e00189 18. <https://doi.org/10.1128/JB.00189-18>.
 29. Krogh, A., Larsson, B., von Heijne, G., and Sonnhammer, E.L.L. (2001). Predicting transmembrane protein topology with a hidden markov model: application to complete genomes. *J. Mol. Biol.* 305, 567–580. <https://doi.org/10.1006/jmbi.2000.4315>.
 30. Holm, L. (2022). Dali server: structural unification of protein families. *Nucleic Acids Res.* 50, W210–W215. <https://doi.org/10.1093/nar/gkac387>.
 31. Picton, D.M., Harling Lee, J.D., Duffner, S.J., Went, S.C., Morgan, R.D., Hinton, J.C.D., and Blower, T.R. (2022). A widespread family of WYL domain transcriptional regulators co-localizes with diverse phage defence systems and islands. *Nucleic Acids Res.* 50, 5191–5207. <https://doi.org/10.1093/nar/gkac334>.
 32. Shmakov, S.A., Makarova, K.S., Wolf, Y.I., Severinov, K.V., and Koonin, E.V. (2018). Systematic prediction of genes functionally linked to CRISPR Cas systems by gene neighborhood analysis. *Proc. Natl. Acad. Sci. USA* 115, E5307–E5316. <https://doi.org/10.1073/pnas.1803440115>.
 33. Shin, H., Lee, J. H., Kim, H., Choi, Y., Heu, S., and Ryu, S. (2012). Receptor Diversity and Host Interaction of Bacteriophages Infecting *Salmonella enterica* Serovar Typhimurium. *PLOS One* 7, e43392. <https://doi.org/10.1371/journal.pone.0043392>.
 34. Ollis, D.L., Cheah, E., Cygler, M., Dijkstra, B., Frolow, F., Franken, S.M., Harel, M., Remington, S.J., Silman, I., and Schrag, J. (1992). The α/β hydrolase fold. *Protein Eng.* 5, 197–211. <https://doi.org/10.1093/protein/5.3.197>.
 35. Choi, K. H., and Schweizer, H.P. (2006). mini Tn7 insertion in bacteria with single attTn7 sites: example *Pseudomonas aeruginosa*. *Nat. Protoc.* 1, 153–161. <https://doi.org/10.1038/nprot.2006.24>.
 36. Hmelo, L.R., Borlee, B.R., Almlad, H., Love, M.E., Randall, T.E., Tseng, B.S., Lin, C., Irie, Y., Storek, K.M., Yang, J.J., et al. (2015). Precision engineering the *Pseudomonas aeruginosa* genome with two step allelic exchange. *Nat. Protoc.* 10, 1820–1841. <https://doi.org/10.1038/nprot.2015.115>.
 37. Qiu, D., Damron, F.H., Mima, T., Schweizer, H.P., and Yu, H.D. (2008). PBAD Based Shuttle Vectors for Functional Analysis of Toxic and Highly Regulated Genes in *Pseudomonas* and *Burkholderia* spp. and Other Bacteria. *Appl. Environ. Microbiol.* 74, 7422–7426. <https://doi.org/10.1128/AEM.01369-08>.
 38. Goodman, A.L., Kulasekara, B., Rietsch, A., Boyd, D., Smith, R.S., and Lory, S. (2004). A Signaling Network Reciprocally Regulates Genes Associated with Acute Infection and Chronic Persistence in *Pseudomonas aeruginosa*. *Dev. Cell* 7, 745–754. <https://doi.org/10.1016/j.devcel.2004.08.020>.
 39. Martin, M. (2011). Cutadapt removes adapter sequences from high throughput sequencing reads. *EMBnet. j.* 17.
 40. Langmead, B., and Salzberg, S.L. (2012). Fast gapped read alignment with Bowtie 2. *Nat. Methods* 9, 357–359. <https://doi.org/10.1038/nmeth.1923>.
 41. Jumper, J., Evans, R., Pritzel, A., Green, T., Figurnov, M., Ronneberger, O., Tunyasuvunakool, K., Bates, R., Židek, A., Potapenko, A., et al. (2021). Highly accurate protein structure prediction with AlphaFold. *Nature* 596, 583–589. <https://doi.org/10.1038/s41586-021-03819-2>.
 42. Emsley, P., Lohkamp, B., Scott, W.G., and Cowtan, K. (2010). Features and development of coot. *Acta Crystallogr. D* 66, 486–501. <https://doi.org/10.1107/S0907444910007493>.
 43. Adams, P.D., Grosse Kunstleve, R.W., Hung, L.W., Ioerger, T.R., McCoy, A.J., Moriarty, N.W., Read, R.J., Sacchettini, J.C., Sauter, N.K., and Terwilliger, T.C. (2002). PHENIX: building new software for automated crystallographic structure determination. *Acta Crystallogr. D* 58, 1948–1954. <https://doi.org/10.1107/S0907444902016657>.
 44. Schäffer, A.A., Aravind, L., Madden, T.L., Shavirin, S., Spouge, J.L., Wolf, Y.I., Koonin, E.V., and Altschul, S.F. (2001). Improving the accuracy of PSI-BLAST protein database searches with composition based statistics and other refinements. *Nucleic Acids Res.* 29, 2994–3005.
 45. Steinegger, M., and Söding, J. (2017). MMseqs2 enables sensitive protein sequence searching for the analysis of massive data sets. *Nat. Biotechnol.* 35, 1026–1028. <https://doi.org/10.1038/nbt.3988>.
 46. Price, M.N., Dehal, P.S., and Arkin, A.P. (2009). FastTree: Computing Large Minimum Evolution Trees with Profiles instead of a Distance Matrix. *Mol. Biol. Evol.* 26, 1641–1650. <https://doi.org/10.1093/molbev/msp077>.
 47. Mateus, A., Bobonis, J., Kurzawa, N., Stein, F., Helm, D., Hevler, J., Typas, A., and Savitski, M.M. (2018). Thermal proteome profiling in bacteria: probing protein state in vivo. *Mol. Syst. Biol.* 14, e8242. <https://doi.org/10.15252/msb.20188242>.
 48. Hughes, C.S., Foehr, S., Garfield, D.A., Furlong, E.E., Steinmetz, L.M., and Krijgsvelde, J. (2014). Ultrasensitive proteome analysis using paramagnetic bead technology. *Mol. Syst. Biol.* 10, 757. <https://doi.org/10.15252/msb.20145625>.
 49. Ritchie, M.E., Phipson, B., Wu, D., Hu, Y., Law, C.W., Shi, W., and Smyth, G.K. (2015). limma powers differential expression analyses for RNA sequencing and microarray studies. *Nucleic Acids Res.* 43, e47. <https://doi.org/10.1093/nar/gkv007>.
 50. Gatto, L., and Lilley, K.S. (2012). MSnbase an R/Bioconductor package for isobaric tagged mass spectrometry data visualization, processing and quantitation. *Bioinformatics* 28, 288–289. <https://doi.org/10.1093/bioinformatics/btr645>.
 51. Lee, B.B., Wehrhahn, C., Westheimer, G., and Kremers, J. (1993). Macaque ganglion cell responses to stimuli that elicit hyperacuity in man: detection of small displacements. *J. Neurosci.* 13, 1001–1009. <https://doi.org/10.1523/JNEUROSCI.13-03-01001.1993>.
 52. Otwinowski, Z., and Minor, W. (1997). Processing of X ray diffraction data collected in oscillation mode. In *Methods Enzymol.*, 276 (Academic Press), pp. 307–326. [https://doi.org/10.1016/S0076-6879\(97\)76066-X](https://doi.org/10.1016/S0076-6879(97)76066-X).
 53. Dutta, S., Watson, B.G., Mattoo, S., and Rochet, J. C. (2020). Calcein Release Assay to Measure Membrane Permeabilization by Recombinant alpha Synuclein. *Bio Protoc.* 10, e3690. <https://doi.org/10.21769/BioProtoc.3690>.
 54. O’Leary, N.A., Wright, M.W., Brister, J.R., Ciufu, S., Haddad, D., McVeigh, R., Rajput, B., Robbertse, B., Smith White, B., Ako Adjei, D., et al. (2016). Reference sequence (RefSeq) database at NCBI: current status, taxonomic expansion, and functional annotation. *Nucleic Acids Res.* 44, D733–D745. <https://doi.org/10.1093/nar/gkv1189>.
 55. Lu, S., Wang, J., Chitsaz, F., Derbyshire, M.K., Geer, R.C., Gonzales, N.R., Gwadz, M., Hunwitz, D.I., Marchler, G.H., Song, J.S., et al. (2020). CDD/SPARCLE: the conserved domain database in 2020. *Nucleic Acids Res.* 48, D265–D268. <https://doi.org/10.1093/nar/gkz991>.
 56. Zimmermann, L., Stephens, A., Nam, S. Z., Rau, D., Kübler, J., Lozajic, M., Gabler, F., Söding, J., Lupas, A.N., and Alva, V. (2018). A Completely Reimplemented MPI Bioinformatics Toolkit with a New HHpred Server at its Core. *J. Mol. Biol.* 430, 2237–2243. <https://doi.org/10.1016/j.jmb.2017.12.007>.
 57. Gao, L., Altae Tran, H., Böhning, F., Makarova, K.S., Segel, M., Schmid Burgk, J.L., Koob, J., Wolf, Y.I., Koonin, E.V., and Zhang, F. (2020). Diverse Enzymatic Activities Mediate Antiviral Immunity in Prokaryotes. *Science* 369, 1077–1084. <https://doi.org/10.1126/science.aba0372>.
 58. Makarova, K.S., Wolf, Y.I., Snir, S., and Koonin, E.V. (2011). Defense Islands in Bacterial and Archaeal Genomes and Prediction of Novel Defense Systems. *J. Bacteriol.* 193, 6039–6056. <https://doi.org/10.1128/JB.05535-11>.

STAR★METHODS

KEY RESOURCES TABLE

REAGENT or RESOURCE	SOURCE	IDENTIFIER
Bacterial and virus strains		
PAO1	Alan Davidson Lab	NCBI: NC 002516.2
PA14	Alan Davidson Lab	NCBI: NC 008463.1
PA14;ΔeljukA	This study	N/A
PA14;ΔeljukB	This study	N/A
PA14;ΔeljukA&B	This study	N/A
PAO1; attTn7::jukA; jukB	This study	N/A
PAO1;attTn7::mCherry jukA;jukB mNeonGreen	This study	N/A
PAO1;attTn7::mCherry jukA;jukB	This study	N/A
PB 1	Alan Davidson Lab	NCBI: NC 011810
14 1	Alan Davidson Lab	NCBI: NC 011703
F8	Alan Davidson Lab	NCBI: NC 007810
phi1214	Alan Davidson Lab	N/A
Lind109	Alan Davidson Lab	NCBI: OQ831730.1
PhiKZ	Alan Davidson Lab	NCBI: AF399011.1
KTN4	Zuzanna Drulis Kawa Lab	NCBI: KU521356.1
omko1	Paul Turner Lab	NCBI: ON631220.1
phiPA3	Alan Davidson Lab	NCBI: NC 028999.1
EL	Alan Davidson Lab	NCBI: NC 007623.1
PA5oct	Rob Lavigne Lab	NCBI: MK797984
M6	Peter Weigele	NCBI: NC 007809
YuA	Rob Lavigne Lab	NCBI: NC 010116
PA 1	Peter Weigele	NCBI: MN504636.1
D3	Alan Davidson Lab	NCBI: AF165214
DMS3	Alan Davidson Lab	NCBI: DQ631426.1
JBD18	Alan Davidson Lab	NCBI: JX495041.1
JBD25	Alan Davidson Lab	NCBI: JX495042.1
JBD30	Alan Davidson Lab	NCBI: NC 020198.1
JBD68	Alan Davidson Lab	NCBI: KY707339.1
KMV	Rob Lavigne Lab	NCBI: AJ505558
PaMx33	Gabriel Guarneros Peña Lab	NCBI: KU884561
PaMx35	Gabriel Guarneros Peña Lab	NCBI: KU884562
PaMx41	Gabriel Guarneros Peña Lab	NCBI: NC 055711.1
PaMx43	Gabriel Guarneros Peña Lab	NCBI: KU884564.1
Pf4	Paul Bollyky Lab	Locus ID in PAO1: PA0715 to PA0729
Luz19	Rob Lavigne Lab	NCBI: AM910651
Luz7	Rob Lavigne Lab	NCBI: NC 013691.1
LKD16	Rob Lavigne Lab	NCBI: AM265638
Chemicals, peptides, and recombinant proteins		
PaJukA	This study	N/A
PaJukB	This study	N/A
gp241	This study	N/A
PaJukA (R73A, K74A)	This study	N/A

(Continued on next page)

Continued

REAGENT or RESOURCE	SOURCE	IDENTIFIER
gp241 ²⁴⁻¹⁰⁹	This study	N/A
SxJukB	This study	N/A
Critical commercial assays		
Deasy UltraClean Microbial Kit	Qiagen	Cat# 10196 4
Turbo DNA free kit	Invitrogen	Cat# AM1907
Luna® Universal One Step RT qPCR Kit	NEB	Cat# E3005L
PerfeCTa® SYBR® Green SuperMix	QuintaraBio	Cat# 95054 500
SMARTer Stranded RNA Seq kit	Takara	Cat# 634837
AMPure XP beads	Beckman Coulter	Cat# A63881
End It DNA End Repair Kit	Biosearch Technologies	Cat# ER0720
DNA Clean and Concentrator kit	Zymo Research	Cat# D4034
Fast Link™ DNA Ligation Kit	Biosearch Technologies	Cat# LK0750H
Zyppy Plasmid Miniprep kit	Zymo Research	Cat #ZD4037
cOmplete protease inhibitor cocktail	Roche	Cat# 11697498001
TMT10plex	Thermo Fisher Scientific	Cat# 90111
Deposited data		
Structure of SxJukB	This study	PDB: 9JHT
Proteomics data	This study	PRIDE: PXD052338
Oligonucleotides		
See Table S4 for primers used for PA14 transposon mutant screen	This study	N/A
See Table S4 for primers used for qPCR and RT qPCR	This study	N/A
Recombinant DNA		
pUC18T mini Tn7T	Choi and Schweizer ³⁵	N/A
pTNS3	Choi and Schweizer ³⁵	N/A
pFLP2	Choi and Schweizer ³⁵	N/A
pMQ30	Hmelo et al. ³⁶	N/A
pHERD20T	Qiu et al. ³⁷	N/A
pHERD30T	Qiu et al. ³⁷	N/A
pBTK30	Goodman et al. ³⁸	N/A
pMQ30 PA14;deljukA	This study	N/A
pMQ30 PA14;deljukB	This study	N/A
pMQ30 PA14;deljukA&B	This study	N/A
miniTn7 PAO1; attTn7::jukA; jukB	This study	N/A
miniTn7 PAO1;attTn7::mCherry2 jukA;jukB mNeonGreen	This study	N/A
miniTn7 PAO1;attTn7::mCherry2 jukA;jukB	This study	N/A
p30T pBAD::JukA	This study	N/A
p30T pBAD::JukB	This study	N/A
p30T pBAD::JukAB	This study	N/A
p30T native promoter::JukAB	This study	N/A
p30T pBAD::mCherry jukA	This study	N/A
p30T pBAD::jukB mNeonGreen	This study	N/A
p20T mCherry jukA;jukB mNeonGreen	This study	N/A
B1	This study	N/A
C1	This study	N/A

(Continued on next page)

Continued

REAGENT or RESOURCE	SOURCE	IDENTIFIER
F1	This study	N/A
C1; delkz241	This study	N/A
C1; delkz242	This study	N/A
C1; delkz241 242	This study	N/A
F1; delkz241	This study	N/A
F1; delkz242	This study	N/A
F1; delkz241 242	This study	N/A
p30T pBAD::kz241	This study	N/A
p30T pBAD::kz242	This study	N/A
p30T pBAD::kz241 242	This study	N/A
C1; kz241 mNeonGreen	This study	N/A
C1; kz241 delTM mNeonGreen	This study	N/A
p20T mCherry jukA;jukB mNeonGreen JukA DD(19,20)AA	This study	N/A
p20T mCherry jukA;jukB mNeonGreen JukA HPE(46 48)AAA	This study	N/A
p20T mCherry jukA;jukB mNeonGreen JukA NS(66,67)AA	This study	N/A
p20T mCherry jukA;jukB mNeonGreen JukA K89A	This study	N/A
p20T mCherry jukA;jukB mNeonGreen JukA K240A	This study	N/A
p20T mCherry jukA;jukB mNeonGreen JukA KR(43,44)AA	This study	N/A
p20T mCherry jukA;jukB mNeonGreen JukA RK(73,74)AA	This study	N/A
p20T mCherry jukA;jukB mNeonGreen JukA ED(81,85)AA	This study	N/A
p20T mCherry jukA;jukB mNeonGreen JukA R197A	This study	N/A
p20T mCherry jukA;jukB mNeonGreen JukA R238A	This study	N/A
p20T mCherry jukA;jukB mNeonGreen JukA E104A	This study	N/A
p20T mCherry jukA;jukB mNeonGreen JukA C230A	This study	N/A
p20T mCherry jukA;jukB mNeonGreen JukA Y79A	This study	N/A
p20T mCherry jukA;jukB mNeonGreen JukA R225A	This study	N/A
pET22b PaJukA purification	This study	N/A
pET22b PaJukA(R73A,K74A) purification	This study	N/A
pET28a PaJukB purification	This study	N/A
pET28a gp241 purification	This study	N/A
pET28a gp241 ²⁴⁻¹⁰⁹ purification	This study	N/A
pRSFDuet SxJukB purification	This study	N/A
p30T pBAD::mCherry SxjukA; SxjukB mNeonGreen	This study	N/A
p30T pBAD::H _p juk	This study	JukA: WP 000394882.1; NA: WP 079993045.1

(Continued on next page)

Continued

REAGENT or RESOURCE	SOURCE	IDENTIFIER
p30T pBAD:: <i>Jsjuk</i>	This study	JukA: WP 096234085.1; XRE: WP 157750926.1
p30T pBAD:: <i>Dsjuk</i>	This study	JukA: WP 176630659.1; JukB: WP 176630660.1
p30T pBAD:: <i>Vtjuk</i>	This study	JukA: WP 162046516.1; JukA: WP 162046517.1; JukB: WP 197739562.1
p30T pBAD:: <i>Fkjuk</i>	This study	JukA: WP 144076013.1; JukB: WP 144076012.1
p30T pBAD:: <i>Jzjuk</i>	This study	JukA: WP 130590268.1; JukB: WP 130590269.1
p30T pBAD:: <i>Smjuk</i>	This study	JukA: WP 049408735.1; JukB: WP 049408736.1
p30T pBAD:: <i>Avjuk</i>	This study	JukA: WP 182927789.1; NA: WP 182927788.1
p30T pBAD:: <i>Capnocytophaga juk</i>	This study	JukA: WP 106095579.1; NA: WP 106095580.1
p30T pBAD:: <i>Sxjuk</i>	This study	JukA: WP 224020616.1; JukB: WP 224020615.1
p30T pBAD:: <i>Rcjuk</i>	This study	JukA: WP 012565274.1; JukB: WP 012565275.1
p30T pBAD:: <i>Hcjuk</i>	This study	JukA: WP 014666958.1
p30T pBAD:: <i>Psjuk</i>	This study	JukA: WP 201417792.1; NA: WP 201417793.1
p30T pBAD:: <i>Lpjuk</i>	This study	JukA: WP 207291724.1; JukB: WP 207291725.1
p30T pBAD:: <i>Vajuk</i>	This study	JukA: BCB42114.1; HTH: BCB42115.1
p30T pBAD:: <i>Kqjuk</i>	This study	DUF2541: WP 227506502.1; JukA: WP 048322949.1
p30T pBAD:: <i>Pfjuk</i>	This study	JukA: WP 159957406.1
p30T pBAD:: <i>Emjuk</i>	This study	JukA: WP 121372120.1; XRE: WP 121372119.1

Software and algorithms

Cutadapt	Martin ³⁹	https://cutadapt.readthedocs.io/en/stable/
Bowtie	Langmead and Salzberg ⁴⁰	https://bowtie.bio.sourceforge.net/bowtie2/index.shtml
Nikon Elements AR software		N/A
R Studio		https://posit.co/download/rstudio/desktop/
MSFragger		https://msfragger.nesvilab.org/
AlphaFold2	Jumper et al. ⁴¹	https://colab.research.google.com/github/sokrypton/ColabFold/blob/main/AlphaFold2.ipynb
COOT	Emsley et al. ⁴²	https://www2.mrc-lmb.cam.ac.uk/personal/pemsley/coot/
PHENIX	Adams et al. ⁴³	https://phenix-online.org/
PSI BLAST	Schäffer et al. ⁴⁴	N/A
MMseqs2	Steinegger and Söding ⁴⁵	https://github.com/soedinglab/MMseqs2
FastTree	Price et al. ⁴⁶	https://morgannprice.github.io/fasttree/

EXPERIMENTAL MODEL AND STUDY PARTICIPANT DETAILS

Pseudomonas aeruginosa strains

Bacterial strains and plasmids used in this study are listed in the [key resources table](#). *P. aeruginosa* strains PAO1, PA14, and their derivatives were grown in LB at 37 °C with aeration at 300 rpm. When necessary, plating was performed on LB agar with carbenicillin (250 µg/ml, for plasmid pHERD20T³⁷) or gentamicin (50 µg/ml, for plasmids pMQ30, pHERD30T, and pUC-miniTn7). Gene expression from pBAD promoters in *P. aeruginosa* is generally leaky and thus was not induced by inducer molecules unless it was noted otherwise.

Bacterial strains for protein purification

All the proteins were expressed in *E. coli* strain BL21 (DE3). Overnight culture was used to inoculate fresh medium at 1:100 dilution. The inoculated culture was grown at 37 °C and 200 rpm until the culture reached an OD₆₀₀ measurement of 0.8. The culture was subsequently induced by 0.2 mM isopropyl-β-D-thiogalactopyranoside (IPTG) and grown at 18 °C and 200 rpm for 12 hours. Cells were harvested via centrifugation at 4500 rpm for 30 minutes. Cell pellets were then flash-frozen in liquid nitrogen, and stored at -20 °C.

Bacteriophages

Phages used in this study are listed in the Key Resource Table. For high-titer phage lysates, PAO1 overnight culture was diluted 100-fold in fresh LB media and infected with phages at MOI 0.01. Phages were collected after overnight infection. Phage stocks were stored at 4 °C and used for routine infection assays.

METHOD DETAILS

Bacterial transformation

Plasmids are delivered into PAO1 with electroporation. While conjugation between PA14 and plasmid-carrying *E. coli* SM10λpir is used to deliver plasmids into PA14. The conjugated cell mixture containing PA14 and SM10 was streaked out on Vogel-Bonner minimal medium (VBMM) agar containing appropriate antibiotics. VBMM media selects against *E. coli* SM10 cells and antibiotics selects against PA14 cells that do not contain the desired plasmid.³⁶

Genetic manipulation

For chromosomal insertions at the attTn7 locus, PAO1 cells were electroporated with the integrating vector pUC18T-mini-Tn7T and the transposase expressing helper plasmid pTNS3, and selected on gentamicin. Potential integrants were screened by colony PCR with primers PTn7R and PglmS-down. Electrocompetent cell preparations, transformations, integrations, selections, plasmid curing and FLP-recombinase-mediated marker excision with pFLP were performed as described previously.³⁵

Two-step allelic exchange was used to delete *jukA*, *jukB*, or *jukAB* from the PA14 genome. Empty vector pMQ30 was used to construct allelic exchange vectors via Gibson Assembly. The allelic exchange vectors were then transformed into PA14 via conjugation. After first-crossover, which occurs shortly after conjugation, VBMM agar containing 50 µg/mL gentamicin was used to select for PA14 merodiploids. Subsequently, sucrose counter-selection was used to select for double crossovers. Sucrose-resistant colonies were then subject to gentamicin to select for sucrose-resistant and antibiotic-sensitive colonies as successful outcomes. The desired colonies are further confirmed via PCR amplification and Sanger sequencing. The protocol is detailed in Hmelo et al.³⁶

To construct strains for microscopy, the N terminus of JukA and its homologs were fused to the mCherry protein and the C terminus of JukB and gp241 were fused to the mNeonGreen protein. The two parts of each fusion protein were connected by a GGGGS linker.

Phage plaque assays

100 µl of appropriate overnight bacterial culture was suspended in 3 ml of 0.45% molten top agar and then poured onto an LB agar plate containing 10 mM MgSO₄ and appropriate antibiotics. After 10-15 min at room temperature, 2 µl of ten-fold serial dilutions of phages was spotted onto the solidified top agar. Plates were incubated overnight at 37 °C.

Growth curve experiments

Growth curve experiments were carried out in a Synergy H1 microplate reader (BioTek, with Gen5 software). Cells were diluted 1:100 from a saturated overnight culture with 10 mM MgSO₄ and antibiotics and inducers, as appropriate. Diluted culture (140 µl) was added together with 10 µl of phage to wells in a 96-well plate. This plate was cultured with maximum double orbital rotation at 37 °C for 24h with OD₆₀₀ nm measurements every 5 minutes.

PA14 Transposon mutant library Screening

Construction of PA14 Tn mutant library

Transposon (Tn) insertion mutants were generated by mating PA14 and *E. coli* SM10λpir carrying the suicide vector pBTK30.³⁸ The mini-transposon pBTK30 is a suicide delivery vector (ori R6K) that contains a mariner C9 transposase, an origin of transfer (oriT RK2),

and a β -lactamase gene (*bla*) specifying ampicillin resistance. The 1.5-kilobase transposable element is located between 28 base pair inverted repeats and consists of an *aacC1* gene (providing gentamicin resistance) that is transcribed toward a transcriptional and translational terminator. Successfully conjugated PA14 cells were selected for on VBMM agar containing 50 μ g/ml gentamicin. The selected PA14 cells contain Tn insertions at random sites in the genome. \sim 200,000 mutant colonies were collected and pooled together. The pool of PA14 Tn mutant library was aliquoted and stored at -80°C at 10^{10} cells/ml.

Phage treatment

\sim 10⁹ PA14 Tn mutant cells (\sim 10,000 cells/mutant) were removed from -80°C , diluted 30-fold into fresh LB media containing 50 μ g/ml gentamicin and 10 mM MgSO₄, and recovered at 37°C , 300 rpm for 2 hours. Five 100 μ l replicates were aliquoted from the recovered mutant library with one replicate treated with ϕ KZ at MOI 5 as the MOI5 infection sample, two treated with SM buffer as non-infection controls, and two collected as samples at time 0. The rest of the recovered mutant library was diluted three-fold with the same media. Four 100 μ l replicates were aliquoted from the diluted mutant library with two replicates treated with ϕ KZ at MOI 30 as the MOI30 infection samples and the other two treated with SM buffer as the corresponding non-infection controls. The infection samples and non-infection controls were immediately grown at 37°C and 300 rpm in a 96-well plate with their OD600 measurements being monitored. Cells were collected via centrifugation after \sim 5 hours of treatment.

Genome extraction and library preparation

Genome extraction was conducted using Qiagen Deasy UltraClean Microbial Kit. \sim 1 μ g genomic DNA from each sample was used to construct the sequencing library using NEB Illumina Library Prep Kit. Customized primers carrying unique multiplexing tags and multiplexing indices were designed and used for adaptor ligation and library amplification. Primer YL001 was annealed to YL002, YL003, YL004, or YL005 and used as the adaptor in the adaptor ligation step. The downstream transposon junctions were amplified using a two-step PCR protocol with the second step as a nested PCR reaction to reduce nonspecific PCR amplification. Primer sequences are included in Table S4.

Sequencing and analysis

DNA libraries were sequenced using Illumina next-seq technology with >2 million reads per sample. Sequencing data were trimmed using the software Cutadapt³⁹ and aligned to the reference genome (NC002516.2) using Bowtie.⁴⁰ Transposon junctions were extracted. The number of reads for each transposon junctions was counted. Assuming that transposon insertions within the same gene shared similar phenotypes, we treated mutations within the same gene as a mutant group, referred to the mutant group as “mutant” hereafter. Note that only mutants with Tn insertions in the coding regions were considered in our analysis.

Next, to evaluate the effect of bacterial genes in ϕ KZ infection, we compared the frequency of mutants in the presence and absence of ϕ KZ infection and calculated their fitness using the equation: $s = \ln('MutantFreq\ W/\ \phi KZ' / 'MutantFreq\ W/O\ \phi KZ')$. If a gene is important in ϕ KZ resistance, disrupting this gene should make bacterial more susceptible to ϕ KZ infection, leading to a lower mutant frequency in the presence of ϕ KZ infection and thus resulting in a negative fitness estimate.

Most mutants did not affect ϕ KZ resistance/sensitivity and had a fitness centered around 0. The fitness distribution of neutral mutants is roughly Gaussian where mutants with a low read number heavily contribute to the left and right tail of the Gaussian distribution. Mutants outside of the Gaussian distribution are likely to be “non-neutral” mutants that affect ϕ KZ infection.

Calling and verification of candidate genes

Two filters were used in our data analysis to call out candidate immune genes. First, genes with low read number across all tested conditions (9 conditions in total including non-infected controls) are likely essential genes whose disruption leads to cell lethality. By removing genes with read number <4000 across all conditions, 4458 genes are left, which is comparable to the 4469 non-essential genes recovered in the curated PA14 mutant library.¹⁸ Second, the library was treated with ϕ KZ at MOI30 and MOI5 with MOI30 treatment resulting in robust killing of PA14 wild-type cells. We removed strains with fitness >-1.1 at MOI 30 (p -value 0.05) as a strict cutoff and fitness >-0.6 at MOI5 as a loose cutoff (p -value = 0.21). With above two filters applied, 10 potential candidate genes were left with 9 out of them, including *jukA* and *jukB*, present in the arrayed PA14 Tn mutant library.

Adsorption assay

Adsorption assays were conducted by infecting exponentially growing bacteria with phage at MOI 0.01 in a flask. Infected bacteria cultures were grown at 37°C with gentle shaking at 60–80 rpm. For each timepoint, 50 μ l of samples were removed from the flask and added to 450 μ l of SM buffer containing extra chloroform. Samples were then centrifuged at 5000 \times g for 5 minutes and the supernatants were used to quantify plaque forming units.

Fluorescence microscopy and imaging

Agarose pad preparation

LB containing 10 mM MgSO₄ will be referred to as LBM. 0.064 gram of agarose were added into a mixture of 2 ml LBM and 6 ml H₂O, melted and kept at 55°C . DAPI was added to the melted gel liquid to reach a final concentration of 0.5 μ g/ml. The gel liquid was poured onto assembled slides to form agar pads.

Cell preparation

Overnight bacterial culture was diluted 100-fold into fresh LBM. The inoculated cells were grown at 37°C with aeration at 300 rpm until reaching OD600 \sim 0.4. In cases where phage infection was needed, cell culture and phages were mixed to a desired MOI and incubated in a dry block at 30°C for 10 minutes. 1 μ l of bacterial cell or bacterial and phage mixture were added onto a piece of

agarose pad and assembled onto slides for imaging. Note that *jukB* expression is ~80 fold higher than the chromosomal integrated operon when being expressed on the pHERD30T plasmid and induced by 0.1% arabinose, which leads to JukB aggregation. To avoid artificial protein aggregation, arabinose was not added when imaging cells that contained plasmids expressing *jukA* and *jukB*. The leaky expression was confirmed to be functional.

Imaging

Microscopy was performed on an inverted epifluorescence (Ti2-E, Nikon, Tokyo, Japan) equipped with the Perfect Focus System (PFS) and a Photometrics Prime 95B 25-mm camera. Image acquisition and processing were performed using Nikon Elements AR software.

qPCR and RT-qPCR

Bacteria was grown to the log phase with an OD₆₀₀ measurement of ~0.4 and infected with ϕ KZ to desired MOIs. 500 μ l of cell culture were removed at each timepoint. Cell pellets were immediately collected by spinning down the cell culture at 6000 x g. For RNA extraction, cell pellets were flash-frozen using liquid nitrogen and stored at -80 °C. For DNA extraction, cell pellets were stored at -20 °C directly. Total RNA was extracted from the resulting cell pellets by performing acidic phenol-chloroform extractions. DNA was removed from the RNA extracts by Invitrogen Turbo DNA-free kit (Cat. No. AM1907). Luna® Universal One-Step RT-qPCR Kit from NEB was used for RT-qPCR reactions. Genomic DNA was extracted using standard phenol-chloroform DNA extraction protocol. PerfeCTa® SYBR® Green SuperMix from QuantaBio was used for qPCR reactions. Both qPCR and RT-qPCR reactions were performed on CFX Connect thermocycler from Bio-Rad. *Pseudomonas aeruginosa* housing-keeping gene *rpoD* was used as the internal control during calculation. For qPCR measurements, gene fold changes were normalized against the readout for time 0 samples. Primers used for qPCR and RT-qPCR are included in Table S4.

RNA sequencing

Total RNA was extracted as stated above. RNA sequencing libraries were prepared using SMARTer Stranded RNA-Seq kit (Cat. No. 634837) and sequenced via Illumina next-seq technology. Sequencing data were trimmed using the software Cutadapt³⁹ and aligned to ϕ KZ reference genome (AF399011.1) using Bowtie.⁴⁰ Total number of base-pairs mapped to the coding region of each ϕ KZ gene was counted. The frequency of each gene was calculated by normalizing the count of base-pairs mapped to the specific gene against the total number of base-pairs mapped to all ϕ KZ coding regions within the same treatment and the same time point, which is then normalized against the gene length.

JukA and JukB mutagenesis

Around the world PCR was used to introduce mutations to *jukA* or *jukB* with PCR primers carrying the desired mutations. Plasmid pHERD20T-*mCherry-jukA;jukB-mNeonGreen* was used as PCR template.

ϕ KZ gDNA plasmid library construction

DNA shearing and size selection

ϕ KZ Genomic DNA was resuspended in TE buffer (10 mM Tris and 1 mM EDTA at pH 8.0) and was sheared into a target size of 3 kb using Covaris M220 Sonicator, following manufacturer's instructions. Sheared ϕ KZ DNA fragments were size-selected using AMPure XP beads from Beckman Coulter. DNA fragments > 2.4 kb were selected for and resuspended in TE buffer.

End-repair and ligation of DNA fragments

Size selected ϕ KZ gDNA fragments were end repaired with End-It DNA End-Repair Kit from Biosearch Technologies, following the manufacturer's protocol. The end-repaired DNA fragments were cleaned up using the DNA Clean and Concentrator kit from Zymo Research. This end-repair step covert sheared DNA into blunt-ended, phosphorylated DNA that is ready for ligation. The end-repaired DNA was ligated into the NheI site of the cloning vector pHERD30T using the Fast-Link™ DNA Ligation Kit from Biosearch Technologies. The inserted ϕ KZ genes are driven by their own native promoter. The ligated product was transformed into the competent *E. coli* cells XL1-Blue.

Extraction of ϕ KZ gDNA plasmid library

~30,000 *E. coli* colonies were scraped off the plates and used for plasmid extraction using Zyppy Plasmid Miniprep kit from Zymo Research. The extracted plasmids were frozen down as the plasmid library containing ϕ KZ gDNA inserts.

Screening phage factors inducing Juk response

The above ϕ KZ gDNA plasmid library were delivered into the *PAO1; attTn7::mCherry-jukA; jukB-mNeonGreen* strain via electroporation. 480 transformed colonies were picked and inoculated into five 96-well plates with each well containing 800 μ l of fresh LB media and 50 μ g/ml gentamicin. Colonies were grown up overnight. The overnight culture was used for growth-curve experiments with ϕ KZ infection at a MOI of 0.5, an MOI that does not affect the growth of *PAO1; attTn7::mCherry-jukA; jukB-mNeonGreen* strain. Strains showing sensitivity to ϕ KZ infection were further verified by comparing the growth of candidate strains without and with ϕ KZ infection. Strains showing compromised growth only in the presence of ϕ KZ infection were further pursued. Plasmids were extracted from strains of interest using Zyppy Plasmid Miniprep kit. The ϕ KZ gDNA inserts of these plasmids were identified using Sanger sequencing.

Whole proteomics assay

Cell collection and cell lysis

25 mL of exponentially growing bacteria were infected by phages at a MOI of 2.5 for 5 minutes. The infected bacterial cells were immediately pelleted down at 4,000 x g at 4 °C for 5 minutes and washed by 10 mL of PBS. The washed cell pellets were frozen down with liquid nitrogen and stored at -80 °C until further procedures. For cell lysis, cell pellets were resuspended in 100 µl of lysis buffer (1X PBS, 0.8% NP-40, 1.5 mM MgCl₂, 50 µg/µl lysozyme, and 0.1 Unit/µl DNase I) supplemented with cOmplete protease inhibitor cocktail and treated with four freeze/thaw cycles by alternating between liquid nitrogen and a heating block set at 22 °C and 850 rpm. 36 µl of cell lysates was transferred to a fresh Eppendorf tube, mixed with 2 µl of 20% SDS, and incubated at room temperature for 10 minutes with gentle shaking. Three replicates were conducted for each treated condition.

Sample preparation for MS analysis

Proteins were digested using an adapted SP3 procedure.⁴⁷ Briefly, 5 µg protein were mixed with 10 µg of beads in 10 µl 15% formic acid and 30 µl ethanol. After shaking the proteins for 15 minutes at room temperature to allow them to bind to the beads, they were four times cleaned with 70% ethanol. Subsequently, 40 µl of digest solution (consisting of 5 mM chloroacetamide, 1.25 mM TCEP, 200 ng trypsin, and 200 ng LysC in 100 mM HEPES pH 8) was added to the proteins to be digested overnight. After then, the peptides were extracted from the beads and vacuum-dried. The peptides were subsequently redissolved in 10 µl of water and labelled with TMT10plex (Thermo Fisher Scientific) for one hour at room temperature. Four microliters of 5% hydroxylamine were used to quench the reaction, and all of the experimental conditions were combined. The samples were desalted on a Waters OASIS HLB µElution Plate (30 µm), washed twice with 100 µl of 0.05% formic acid, eluted with 100 µl of 80% acetonitrile, and dried under vacuum. Ultimately, samples were separated into six fractions using a reversed-phase C18 system operating at a high pH.⁴⁸

LC-MS measurement and file processing

Samples were analyzed as described previously in a 120min gradient on a Q Exactive Plus (Thermo Fisher).⁴⁷ Raw files were converted to mzML format using MSConvert from ProteoWizard, using peak picking, 64-bit encoding and zlib compression, and filtering for the 300 most intense peaks. Files were then searched using MSFragger (v3.6) in FragPipe (19.0) against FASTA database *Pseudomonas aeruginosa* and *Pseudomonas* phage φKZ proteomes, downloaded from Uniprot, identifiers UP000002438 and UP000002098, respectively, including the two immune proteins JukA and JukB, known contaminants and the reversed protein sequences. The following modifications were included into the search parameters: Carbamidomethylation (C, 57.0215), TMT (K, 229.1629) as fixed modifications; Oxidation (M, 15.9949), Acetylation (protein N-terminus, 42.0106), TMT (peptide N-terminus, 229.1629) as variable modifications. For the full scan (MS1) a mass error tolerance of 20 PPM and for MS/MS (MS2) spectra of 20 PPM was set. For protein digestion, 'trypsin' was used as protease with an allowance of maximum 2 missed cleavages requiring a minimum peptide length of 7 amino acids. The false discovery rate on peptide and protein level was set to 0.01. The standard settings of the FragPipe workflow 'TMT10' were used. The following modifications were made: msfragger.add_topN_complementary: 0, msfragger.misc.fragger.enzyme-dropdown-1: trypsin, msfragger.misc.fragger.precursor-charge-hi: 6, msfragger.search enzyme name 1: trypsin, msfragger.search enzyme nocut 1: P, msfragger.use_topN_peaks: 300, peptide-prophet.run-peptide-prophet: true, tmtintegrator.allow_unlabeled: true, tmtintegrator.dont-run-fq-lq: false, tmtintegrator.unique_gene: 1, tmtintegrator.unique_pep: true.

The mass spectrometry proteomics data have been deposited to the ProteomeXchange Consortium via the PRIDE partner repository with the dataset identifier PXD052338. Unique link: <https://www.ebi.ac.uk/pride/review-dataset/a4b4fadab183427c919bc8682559ccb0>. Project accession: PXD052338. Token: BfydkwMPC557

Data processing and analysis

The raw output files of FragPipe (protein.tsv files) were processed using the R programming language. Contaminants and reverse proteins were filtered out and only proteins that were quantified with at least 2 razor peptides (Razor.Peptides >= 2) were considered for the analysis. Moreover, only proteins which were identified and quantified in 2 out of 3 mass spec runs were kept. 3105 proteins passed the quality control filters. Log₂ transformed raw TMT reporter ion intensities ('channel' columns) were first cleaned for batch effects using the 'removeBatchEffect' function of the limma package⁴⁹ and further normalized using the 'normalizeVSN' function of the limma package (VSN - variance stabilization normalization). Missing values were imputed with the 'knn' method using the 'impute' function of the Msnbase package.⁵⁰ Proteins were tested for differential expression using a moderated t-test by applying the limma package ('lmFit' and 'eBayes' functions). The replicate information was added as a factor in the design matrix given as an argument to the 'lmFit' function of limma. Also, imputed values were given a weight of 0.01 while quantified values were given a weight of 1 in the 'lmFit' function. The t-value output of limma for certain statistical comparisons was analyzed with the 'fdrtool' function of the fdrtool packages⁵¹ in order to extract p-values and false discovery rates (q-values were used). A protein was annotated as a hit with a false discovery rate (fdr) smaller 0.05 and an absolute fold-change of greater 2 and as a candidate with a fdr below 0.2 and an absolute fold-change of at least 1.5.

φKZ genetic editing

Deletion of phage genes from φKZ genome was performed via homologous recombination, where an anti-CRISPR gene was used as a selectable marker to select for successfully modified phage mutants using an RNA-targeting CRISPR-Cas13a system. Detailed protocol has been reported previously.²⁶

Protein expression and purification

The *PajukA*, *PajukB*, *SxjukB*, and *kz241* genes were synthesized by GenScript and codon-optimized for expression in *E. coli*. The full-length *PajukA* gene was amplified by PCR and cloned into pET22b vector in which the expressed JukA protein contains a C-terminal His6 tag. *PajukB* and *kz241* were amplified by PCR and cloned into modified pET28a vectors, in which the expressed protein contains a N-terminal His6-SUMO tag. The full-length *SxjukB* was amplified by PCR and cloned into a modified pRSFDuet vector. Proteins were expressed in *E. coli* strain BL21 (DE3) and induced by 0.2 mM IPTG.

Cells expressing all proteins except *PaJukB* were resuspended in lysis buffer (50 mM Tris-HCl pH 8.0, 500 mM NaCl, 10 mM imidazole and 1 mM PMSF) and lysed by sonication. The cell lysate was centrifuged at 20,000 × g for 50 min at 4 °C to remove cell debris. The supernatant was applied onto a self-packaged Ni-affinity column (2 mL Ni-NTA, Genscript) and contaminant proteins were removed with wash buffer (50 mM Tris pH 8.0, 500 mM NaCl, 30 mM imidazole). The fusion gp241 protein with His6-SUMO tag was digested with Ulp1 at 18 °C for 2 h before elution with wash buffer. His tagged proteins were eluted with His-tag elute buffer (50 mM Tris pH 8.0, 300 mM NaCl, 300 mM imidazole). The eluant of protein was concentrated and passed over a Superdex-200 increase 10/300 GL (GE Healthcare) column in buffer A (10 mM Tris-HCl pH 8.0, 500 mM NaCl and 5 mM DTT), then concentrated by ultrafiltration (Amicon Ultra, EMD Millipore) and stored at -80 °C. For *PaJukB*, cells were resuspended in lysis buffer (50 mM Tris-HCl pH 8.0, 500 mM NaCl, 30 mM imidazole, 5% glycerol and 1 mM PMSF) and lysed by sonication. The cell lysate was centrifuged at 12,000 × g for 30 min at 4 °C. Then, 2% DDM was added to the suspended pellet and incubated for 1 hour. Resuspended cell pellet was centrifuged further for 50 minutes at 18,000 × g. The supernatant was loaded onto Ni-affinity column and the protein was purified in the same approach as gp241, but 0.02% DDM was added to the buffers in the following purification process.

In vitro pull-down assay

The proteins used in the pull-down assay, such as His-tagged *PaJukA*, *PaJukB* and gp241 were first exchanged into the buffer containing 10 mM Tris pH 8.0, 500 mM NaCl, 5 mM DTT, and 0.02% DDM. The purified His-tagged *PaJukA* protein was used to pull down the *PaJukB* and gp241. The His-tagged *PaJukA*, *PaJukB* and gp241 were mixed at a molar ratio of 1:2:10 and incubated at 4 °C for 2 h. After that, the mixture was loaded onto 30 μL of Ni resins and incubated at 4 °C for 1 h. The Ni resins were first washed with buffer containing 50 mM Tris-HCl pH 8.0, 30 mM imidazole, 500 mM NaCl and 0.02% DDM for five times, and then washed with buffer containing 50 mM Tris-HCl pH 8.0, 50 mM imidazole, 500 mM NaCl and 0.02% DDM for three times. Meanwhile, His-tagged *PaJukA* proteins mixed and incubated with *PaJukB* or gp241 separately were used as controls. After the wash step, the resins were added with the 4X SDS-PAGE loading buffer (120 mM Tris-HCl (pH 6.8), 400 mM DTT, 8% (w/v) SDS 0.4% (w/v) bromophenol blue, 40% (w/v) glycerol) and boiled at 100 °C for 5 min. The boiled samples were subjected to SDS-PAGE and visualized by Coomassie blue staining.

Surface Plasmon Resonance binding assay

The SPR analysis for *PaJukB* to *PaJukA* or gp241 was performed using a Biacore 8K (GE Healthcare) at room temperature (25 °C). Equal concentrations of *PaJukA* and gp241 were immobilized on channels of the carboxymethyl dextran-modified (CM5) sensor chip to about 5500 Response Unit (RU) separately. To collect data for kinetic analysis, a series of concentrations of *PaJukB* were injected on the chip at a flow rate of 30 μL/min. *PaJukB* at concentrations of 5 μM, 10 μM, 20 μM, 40 μM, and 80 μM, was used to react with *PaJukA*. *PaJukB* at concentrations of 3.125 μM, 6.25 μM, 12.5 μM, 25 μM, 50 μM, 100 μM, and 200 μM, were used to react with gp241. Proteins were in the binding buffer (20 mM HEPES pH 7.5, 500 mM NaCl, and 0.05% (v/v) Tween-20). The protein-ligand complex was allowed to associate for 60 s and dissociate for 60 s. Data were fit with a model describing a bivalent analyte. Kinetic rate constants were extracted from this curve fit using Biacore evaluation software (GE healthcare).

The SPR analysis for gp241 to *PaJukA* was performed using a Biacore T100 (GE Healthcare) at room temperature (25 °C). The *PaJukA* was immobilized on channels of the carboxymethyl dextran-modified (CM5) sensor chip to about 3900 Response Unit (RU). To collect data for kinetic analysis, a concentration series of gp241 (0.5 μM, 1 μM, 2 μM, 4 μM, and 8 μM) in binding buffer (20 mM HEPES pH 7.5, 500 mM NaCl and 0.05% (v/v) Tween-20) was injected over the chip at a flow rate of 30 μL/min. The protein-ligand complex was allowed to associate for 60 s and dissociate for 120 s. Methods of data processing and mapping software were as described above.

Protein crystallization

The *SxJukB* protein was concentrated to 8 mg/ml. The crystals were grown for 3–4 days with reservoir solution containing 0.15 M Potassium thiocyanate, 0.1 M Sodium cacodylate pH 6.5, and 20% v/v PEG 600 at 18 °C. Crystals were cryoprotected with an additional 20% glycerol and flash frozen in liquid nitrogen.

Data collection and structure determination

All the data were collected at SSRF beamlines BL02U1 and BL19U1, integrated and scaled using the HKL2000 package.⁵² The initial model of *SxJukB* was obtained using AlphaFold2.⁴¹ The structure of *SxJukB* was solved through molecular replacement and refined manually using COOT.⁴² The structure was further refined with PHENIX⁴³ using non-crystallographic symmetry and stereochemistry information as restraints. The final structure was obtained through several rounds of refinement. Structural illustrations were

generated using PyMOL (<https://pymol.org/>). Data collection and structure refinement statistics are summarized in [Table S3](#). The SxJukB structure reported in this study has been deposited in the Protein Data Bank under accession code 9JHT.

Liposome-Calcein leakage assay

The liposome containing calcein was prepared using phosphatidyl ethanolamine (PE) by modifying the protocol in Dutta et al.⁵³ Specifically, 2 mg of PE were dissolved in 4 mL of chloroform in a flat-bottom 500 mL beaker. The beaker was placed in the hood for 2 to 3 hours until chloroform was completely evaporated, and a lipid film was formed at the bottom of the beaker. The lipid film was then rehydrated by adding 3 mL of 80 mmol/L calcein into the beaker. Calcein-containing liposomes were produced by subjecting the beaker to bath sonication at 65°C (300 W for 20 minutes). The lipid/calcein solution was loaded onto a Sephadex G-50 manual column that was pre-equilibrated with 1×PBS (10 mM phosphate and 150 mM NaCl, pH 7.4). Free calcein was separated from the liposomes. 700 μL of intact liposomes were eluted and collected from every 500 μL of lipid/calcein solution that was loaded onto the column. To induce calcein leakage, 2 μL of assayed proteins at specific concentrations were mixed with 98 μL of intact liposomes in a black 96-well plate. The resulting fluorescence was monitored with excitation at 475 nm and emission at 520 nm. The amount of calcein released was calculated as Fractional Permeabilization as follows: $Fractional\ Permeabilization = (I_t - I_0) / (I_{max} - I_0)$, where, I_t is the instantaneous fluorescence emission intensity at time t , I_0 is the initial fluorescence intensity at time 0, and I_{max} is the maximum intensity caused by adding 2 μL of 2% (v/v) TritonX-100.

Selecting *jukA*-containing operons for testing

jukA homologs and their ten neighboring genes (5 upstream and 5 downstream) on bacterial genomes were identified. First, we removed genes that were not in the same operon as *jukA* homologs. Genes in the same operon satisfied two relax criteria: a) genes are on the same strand as *jukA*, and b) genes are within the 50bp of the *jukA* homologs. Second, we used the combination of gene names in the same operon as a unique ID to separate these *jukA* containing operons into different groups. For groups with >8 bacterial genomes, a representative was manually selected. Based on the cost to synthesize the operon and the identity of the putative effector, we eventually chose 18 operons for DNA synthesis and cloning. These chosen operons were cloned under the pBAD promoter on the pHERD30T vector.

Multiple sequence alignment of Juk proteins

Multiple sequence alignments for JukA proteins within *Pseudomonas* were performed using Clustal-Omega with its default setting.

Analysis of JukA and JukB distribution

Identification of *JukA* and *JukB* homologs

PSI-BLAST⁴⁴ search (e-value cut-off was set to 10^{-4} , three iterations, the rest of the parameters remained default) was performed using JukA protein (WP_003137196.1) as a query against a database of complete Refseq genomes (November 2021 release).⁵⁴ The set was further manually refined: a few false positives were discarded, and few false negatives (JukB neighbors) were included in the final set. Same procedure was applied for identification of JukB homologs.

Phylogenetic analyses

JukA sequences were clustered using MMseqs2⁴⁵ with the similarity threshold of 90% identity, and one representative was taken from each cluster for further analysis. Sequences were aligned using a previously described iterative procedure.¹⁶ Based on this alignment, N- and C-terminal domains fused to some of JukA homologs were removed and several short sequences were discarded. The remaining sequences were realigned using the same method. The resulting multiple alignment was further filtered to retain the positions with less than 50% of gaps and homogeneity value greater than 0.1. Approximate maximum likelihood phylogenetic trees for the filtered alignments were built using FastTree (WAG evolutionary model, gamma distributed site rates).⁴⁶ The same program was used to obtain support values.

Genomic neighborhood analysis

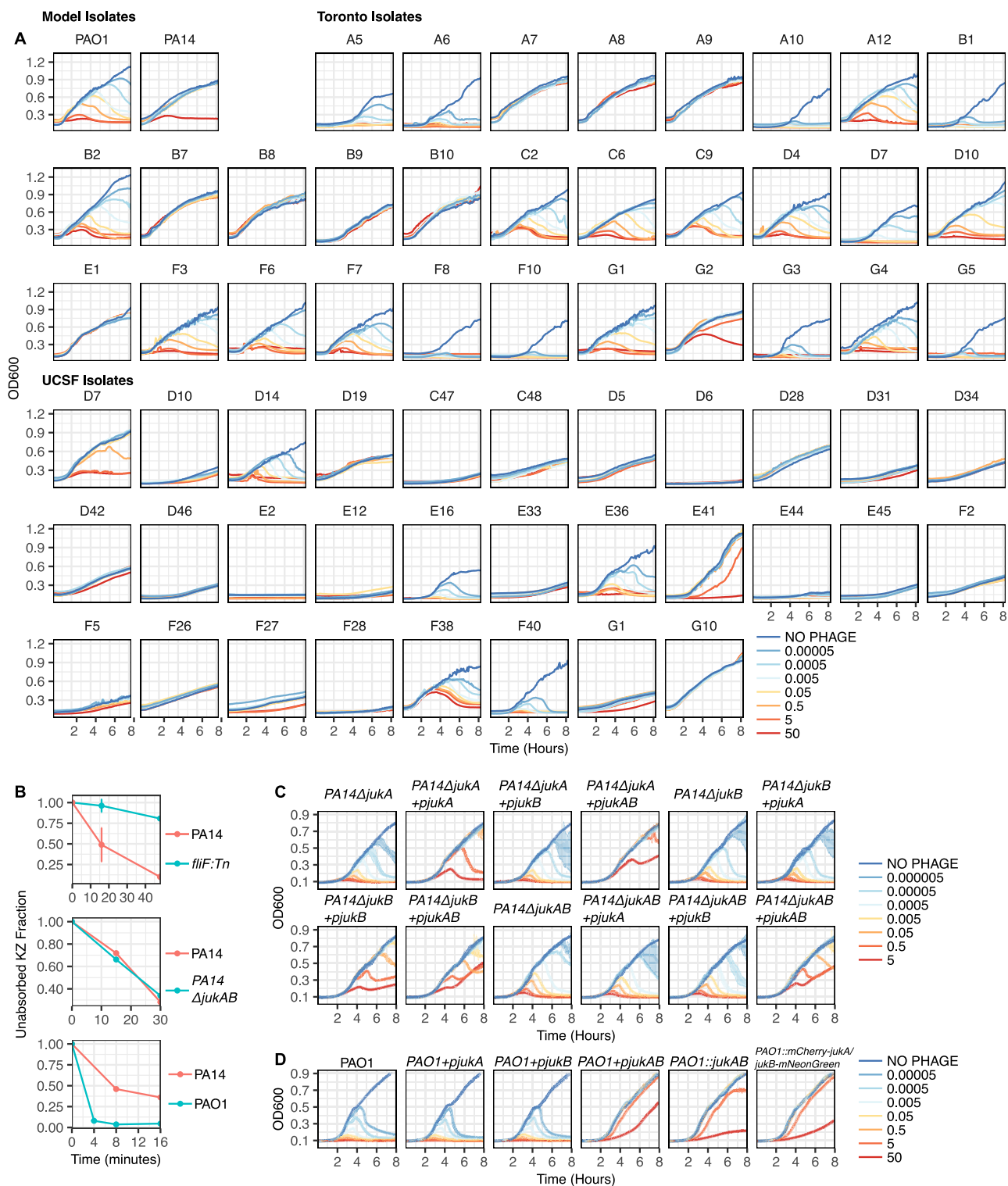
For each representative *jukA* and *jukB* gene used for phylogenetic analysis, 5 genes upstream and downstream were collected and all proteins encoded in these neighborhoods were annotated using PSI-BLAST⁴⁴ with E-value threshold = 0.01 run against position-specific scoring matrices (PSSMs) deposited in the CDD database.⁵⁵ Only hits to regularly updated databases, namely Pfam, CDD and COGs were considered. HHPred search with default parameters against PDB, Pfam and CDD profile databases was used for unannotated proteins or domains.⁵⁶ Additionally, all proteins in the respective neighborhoods were clustered using MMseqs2 program⁴⁵ with the similarity threshold of 0.5, and a cluster identifier was assigned for each ORF in the neighborhood. Defense function was assigned based on CDD annotation and a collection of known and predicted defense system components^{3,57,58} or on the presence of *jukB* genes.

QUANTIFICATION AND STATISTICAL ANALYSIS

Statistical analysis used to interpret the data from PA14 transposon mutant library screening is detailed under the “Calling and verification of candidate genes” subheading in [method details](#). The analysis of the whole proteomics assay is detailed under the “Data

processing and analysis” subheading in [method details](#). Similarly, the methods and analysis used to characterize JukA and JukB distribution are included under the “Analysis of JukA and JukB distribution” subheading in [method details](#). The number of experimental replicates used in this manuscript is reported in relevant figure legends and supplemental figure legends. Standard deviation is plotted in figures and supplemental figures when more than one experimental replicate is involved.

Supplemental figures



(legend on next page)

Figure S1. Discovery and verification of the Juk immune system, related to Figures 1 and 3

(A) Growth curves (measuring OD600) of a panel of *P. aeruginosa* isolates when being infected by phage ϕ KZ at different multiplicities of infection (MOIs). (B) ϕ KZ adsorption efficiency in various *P. aeruginosa* strains. The fraction of unabsorbed phages was plotted as a function of time. Error bar in top panel represents one standard deviation inferred from two biological replicates. Middle and bottom panels contain one replicate. (C and D) Growth curves of indicated strains during ϕ KZ infection. (C) PA14 deletion mutants were complemented by expression of indicated genes in *trans* across a range of MOIs. (D) Growth curves of PAO1 and strains expressing *jukA* (*pjukA*), *jukB* (*pjukB*), or *juk operon* (*pjukAB*) via plasmid and *juk operon* (*PAO1::jukAB*) or fluorescence tagged *juk operon* (*PAO1::mCherry jukA/jukB mNeonGreen*) via chromosome integration. Error bars represent one standard deviation calculated from two technical replicates. The expression of *pjukA* and *pjukB* was induced by 0.1% arabinose.

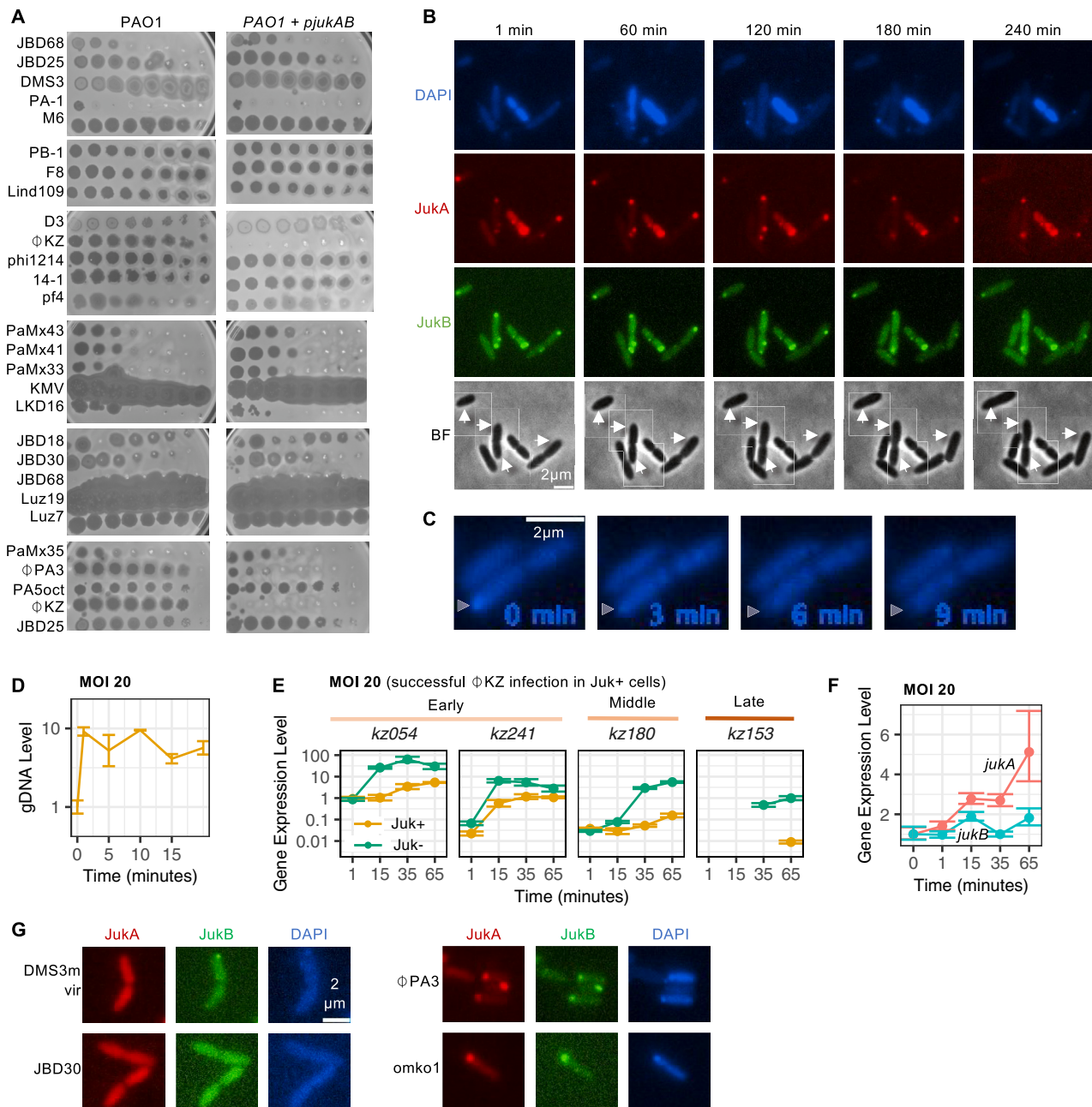


Figure S2. Juk is a non abortive infection immune system specifically targeting early infection of ϕKZ like phages, related to Figures 1, 2, and 3

(A) Phage titration assay with 10 fold phage serial dilutions on indicated bacterial lawns.

(B) Time series visualization of DAPI stained DNA, JukA, JukB, and cells in bright field (BF), using PAO1::mCherry *jukA/jukB* mNeonGreen strain infected by ϕKZ at MOI 1. Cells that were infected by ϕKZ and that also grew/divided over time were labeled by arrows in the bright field images. Since DNA is rapidly cleared, ϕKZ infected cells were inferred via the formation of JukA and JukB puncta (see Figures 3A and 3B).

(C) Time series visualization of ejected ϕKZ genome (pointed by arrows) in Juk+ cells infected by ϕKZ.

(D) Quantification of the DNA level of gene *kz054* over the first 20 min of phage infection (multiplicity of infection is 20) in Juk+ cells.

(E) Transcription levels of ϕKZ early (*kz054* and *kz241*), middle (*kz180*), and late (*kz153*) genes at MOI 20. Points below the assay detection limit were eliminated. Error bar represents one standard deviation inferred from two technical replicates.

(F) Transcription levels of *jukA* and *jukB* before (0 min) and after ϕKZ infection at MOI 20. Transcription levels of *jukA* and *jukB* before infection do not significantly differ from their transcription levels at 65 min post infection (*p* value is 0.24 for *jukA* and 0.26 for *jukB*).

(G) Visualization of JukA, JukB, and DAPI stained DNA, using PAO1::mCherry *jukA/jukB* mNeonGreen cells infected by different phages.

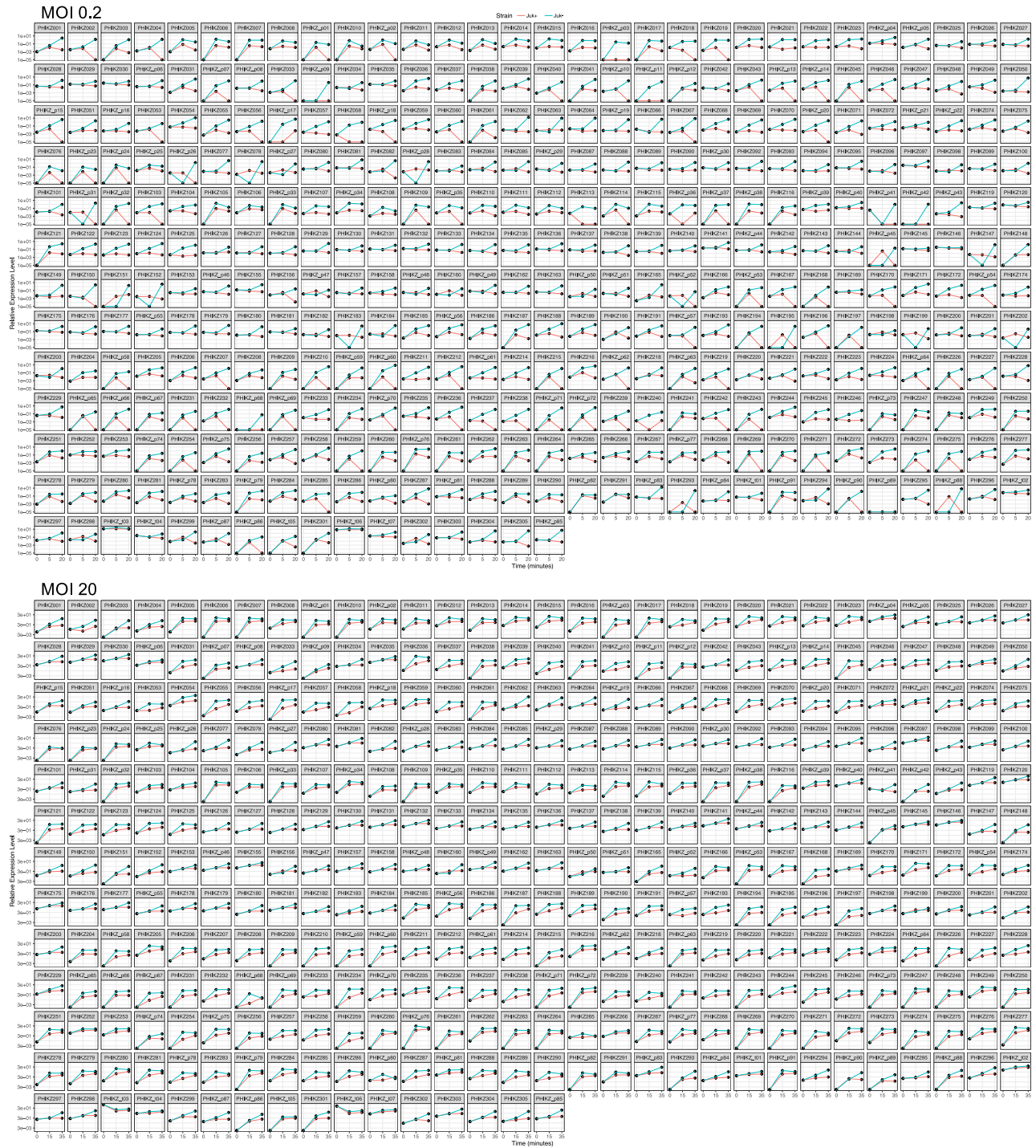


Figure S3. Transcriptome profiling of ϕ KZ genes during infection of Juk expressing cells, related to Figure 2
Whole transcriptome profiling of ϕ KZ at MOIs that lead to failed (MOI 0.2) or successful (MOI 20) infections in Juk+ and Juk- cells.

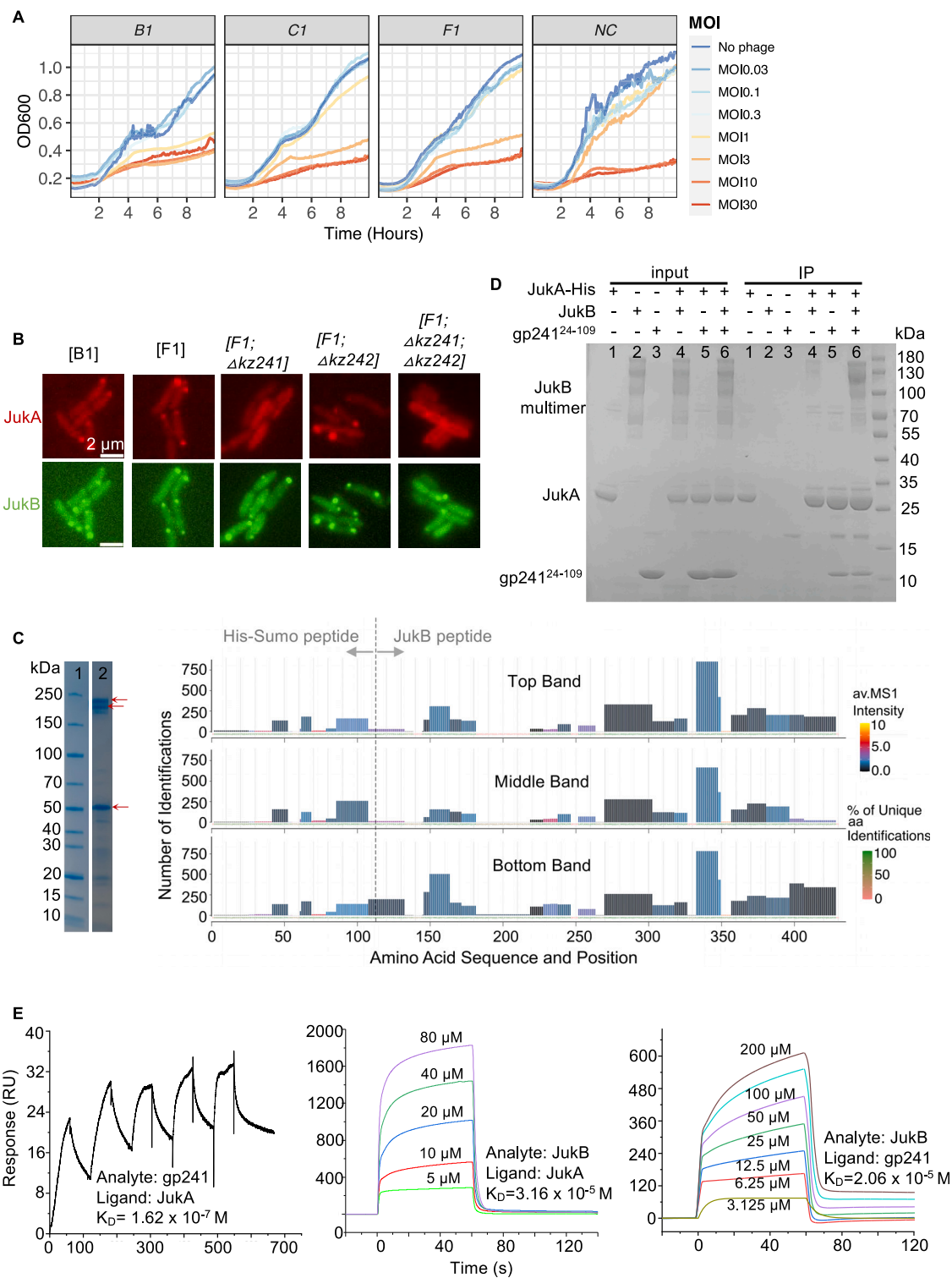


Figure S4. Phage protein gp241 interacts with Juk proteins, related to Figure 4

(A) Bacterial growth curves (OD600) of PAO1:*mCherry jukA/jukB mNeonGreen* strains carrying B1, C1, F1, or negative control (NC) plasmids across a range of MOIs of ϕ KZ.

(B) In the absence of ϕ KZ infection, JukA and JukB localization in PAO1:*mCherry jukA/jukB mNeonGreen* strains carrying wild type B1 or F1 plasmid or F1 plasmid with *kz241*, *kz242*, or *kz241+kz242* deleted.

(legend continued on next page)

(C) Purified His Sumo JukB protein was visualized on SDS PAGE gel by Coomassie staining (right). Three bands from the gel (indicated by arrows), corresponding to the molecular weight of His Sumo JukB tetramer, trimer, and monomer from top to bottom, respectively, were excised and identified as His Sumo JukB peptides via mass spectrometry (left).

(D) *In vitro* immunoprecipitation (IP) assays among purified proteins JukA, JukB, and TM deleted gp241 protein (gp241²⁴⁻¹⁰⁹). JukA contains His tag on its C terminus and is used as the bait protein. + and - indicate that the corresponding protein is and is not added to the reaction.

(E) SPR sensorgrams measured with JukA as the ligand and gp241 as the analyte, JukA as the ligand and JukB as the analyte, and JukB as the ligand and gp241 as the analyte.

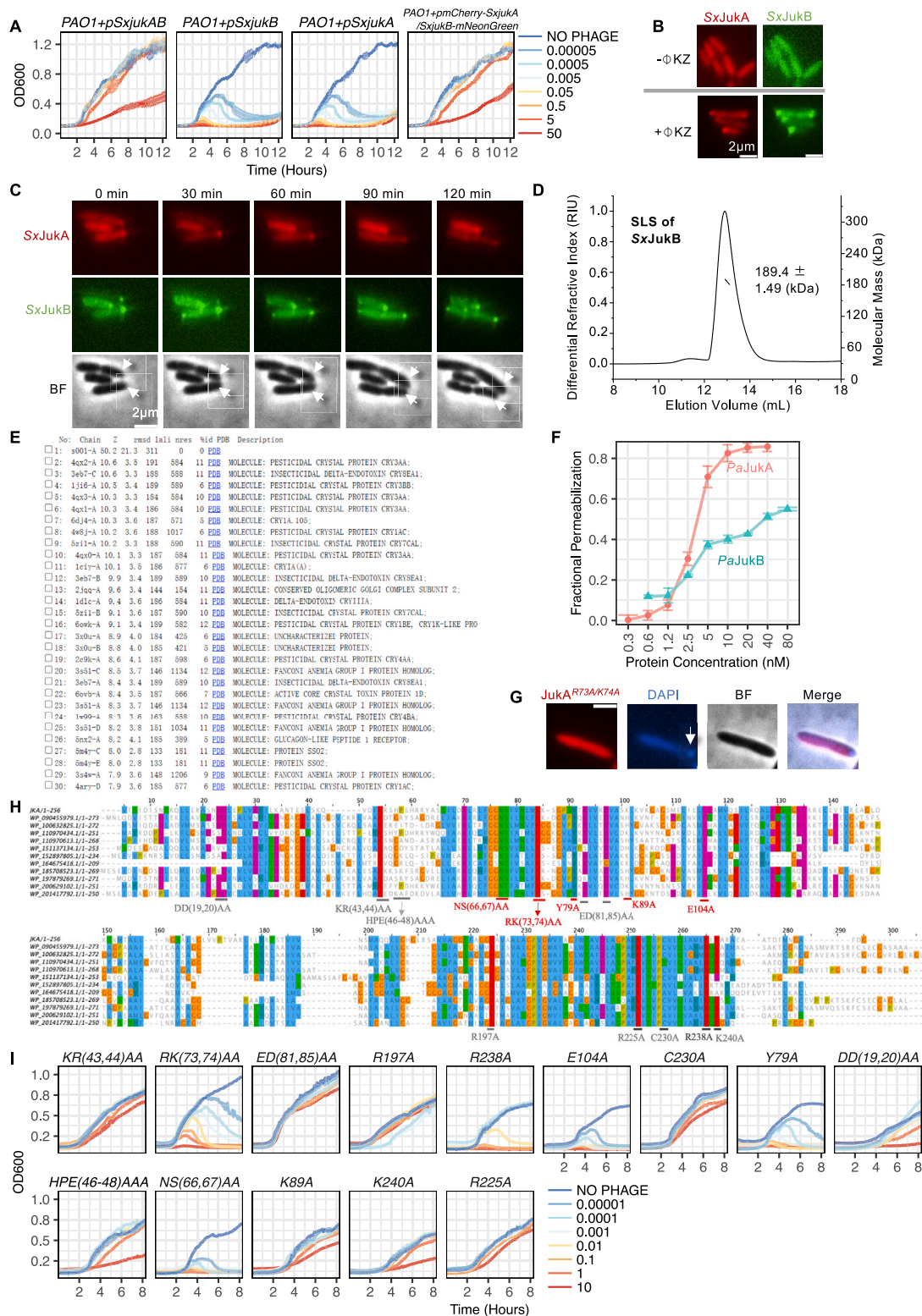


Figure S5. SxJuk behaves similarly to PaJuk, related to Figure 5

(A) Growth curves of PAO1 strains expressing *Sxjuk* operon (*SxjukAB*), *SxjukB*, *SxjukA*, or fluorescence tagged *Sxjuk* operon (*mCherry Sxjuka/SxjukB mNeonGreen*) via plasmid across a range of MOIs of ϕ KZ. Error bars represent one standard deviation calculated from two technical replicates.

(legend continued on next page)

-
- (B) Fluorescence microscopy of SxJukA and SxJukB localization without and with ϕ KZ infection, using PAO1[*pBAD::mCherry Sxjuka/SxjukB mNeonGreen*] strain.
- (C) Time series visualization of SxJukA, SxJukB, and cells in bright field (BF), using PAO1[*pBAD::mCherry Sxjuka/SxjukB mNeonGreen*] cells infected by ϕ KZ at MOI 1. Cells that were infected by ϕ KZ and that also grew/divided over time were labeled by arrows in the bright field images. ϕ KZ infected cells were inferred via the formation of SxJukA and SxJukB puncta.
- (D) Static light scattering measurement of purified SxJukB protein.
- (E) Top hits when searching the SxJukB structure using the Dali search server.
- (F) Fraction of liposomes that are permeabilized at different concentrations of purified PaJukA or PaJukB proteins.
- (G) Visualization of JukA^{R73A/K74A}, DAPI stained DNA, and cell in BF, using ϕ KZ infected PAO1[*pBAD::mCherry jukA^{R73A/K74A}/jukB mNeonGreen*] cells. Ejected ϕ KZ genome is marked by an arrow.
- (H) Multiple sequence alignment of JukA homologs from *P. aeruginosa*. Amino acid residues that were mutated are labeled. Mutations that caused loss of function are in red color.
- (I) Growth curves of PAO1 strains heterologously expressing *juk operon* (*pjukAB*) with indicated *jukA* mutations across a range of MOIs of ϕ KZ.

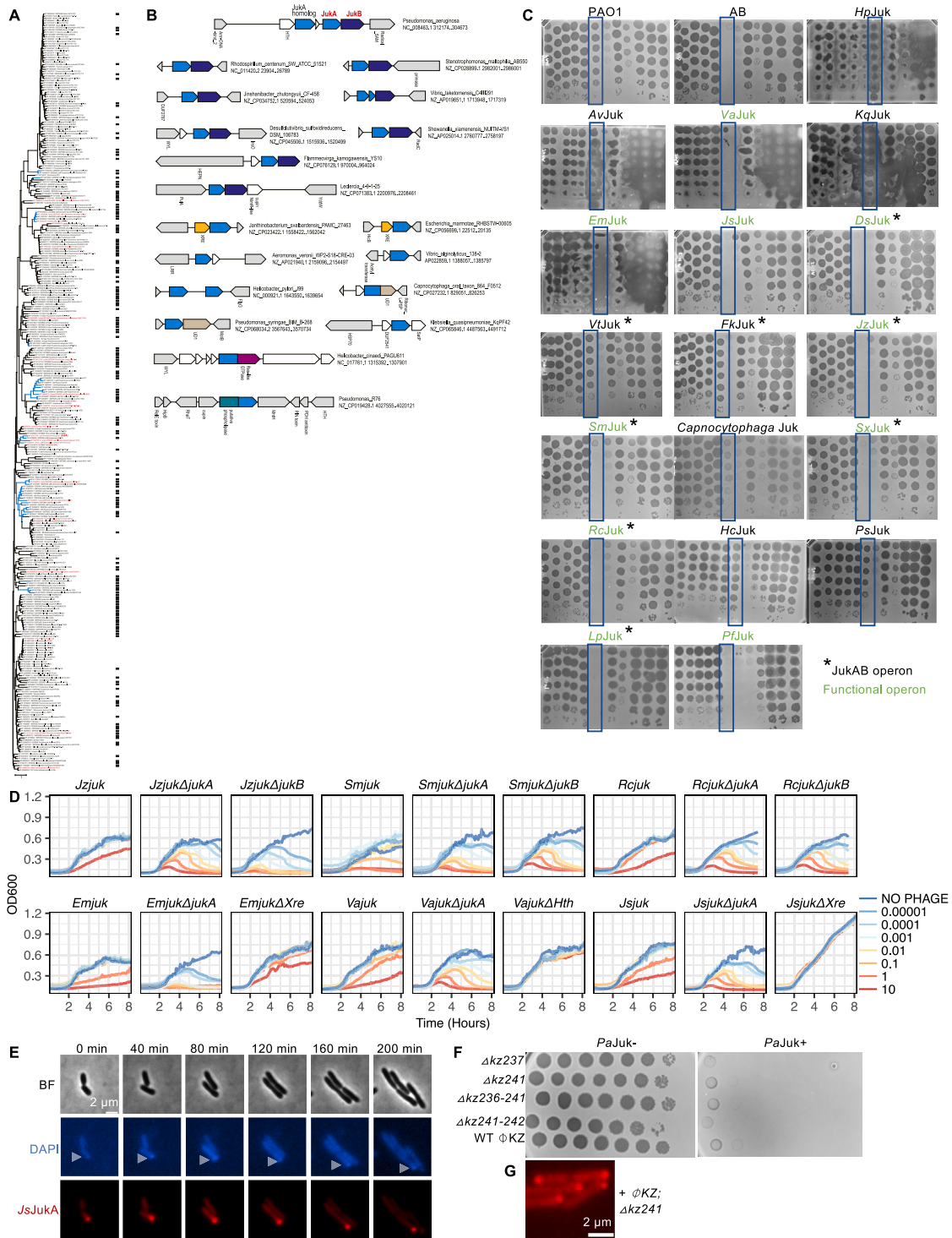


Figure S6. Juk systems encompass numerous, distinct putative effectors in diverse bacteria, related to Figure 6

(A) Phylogenetic tree for 329 representatives of JukA family was built using Fasttree program as described in STAR Methods. The branches leading to JukB present in the same locus as respective JukA are colored blue. Each leaf is denoted by protein identifier, species name, and additional information as follows: DEFENSE at least one known or predicted defense gene is encoded in the respective locus; JukB JukB is encoded in respective locus; a/b hydrolase (patatin homolog), Ras like GTPase, TerB, Zn finger if respective domains are fused to JukA; UD1 is an unknown domain either fused or encoded in the respective JukA locus. Presence of defense genes is also shown by black rectangles on the right. JukA proteins that were experimentally tested are highlighted by red.

(legend continued on next page)

(B) Neighborhood of 18 *JukA*-containing operons that were tested in PAO1. Genes are shown as arrows. Genes and untranslated regions are proportional for their size. Species name, nucleotide accession, and coordinates of respective region are indicated on the right. Homologous genes or domains are shown by the same color. Only genes or domains that are often associated with *jukA* are colored. White arrows—genes that do not have any annotation. Gray arrows—flanking genes. Short names for genes or protein families are indicated below the arrows if annotation is available. Abbreviations for short names: WYL—is ligand binding domain of WYL family, often fused to a DNA binding domain; HEPN—protein containing predicted ribonuclease of HEPN family; UD1—unknown domain 1; HTH—helix-turn-helix; XRE—helix-turn-helix of *xre* family; HNH and PD-DExK are DNA nuclease of respective families.

(C) Immunity function of different *jukA*-containing operons when being expressed in PAO1. Spot titration plaque assays with 10-fold serial dilutions from top to bottom on lawns expressing *jukA*-containing operons from various bacteria. From left to right, the infecting phages are PB-1, 14-1, F8, ϕ 1214, Lind109, ϕ KZ, EL, ϕ PA3, PA5oct, M6, YuA, and PA-1. ϕ KZ is highlighted in the rectangle. 0.1% of arabinose was added to both bottom and top agar to induce the expression of tested *Juk* operons. Operons that have immune function are labeled in green color. Operons consisting of *jukA* and *jukB* homologs are marked with asterisks.

(D) Growth curves of PAO1 strains expressing indicated operons or genes via plasmid across a range of MOIs of ϕ KZ. Gene expression was induced by 0.1% of arabinose.

(E) Time series visualization of cells in bright field (BF), DAPI-stained DNA, and *JsJukA*, using PAO1 cells expressing *mCherry-JsjukA*. Ejected ϕ KZ genomes are marked by arrows.

(F) Titration (10-fold serial dilutions) of wild-type ϕ KZ and its mutants on indicated bacterial lawns.

(G) *JukA* localization in PAO1::*mCherry-jukA/jukB* strain when being infected by ϕ KZ; Δ *kz241* phage mutants. In (E) and (G), MOI 1 is used for ϕ KZ infection.